Transonic Correction Method for Flight Dynamic Stability Analysis of Mach 0.745 Transonic Truss-Braced Wing

Nhan Nguyen*
NASA Ames Research Center, Moffett Field, CA 94035
Juntao Xiong†
KBR Wyle, Inc., Moffett Field, CA 94035

This paper presents a transonic correction method for obtaining dynamic stability derivatives for flight dynamic stability analysis. The method provides a transonic correction to the Theodorsen's theory of unsteady aerodynamics using FUN3D CFD solver of unsteady Reynolds-averaged Navier-Stokes equations (RANS) for a series of wing sections of the Mach 0.745 Transonic Truss-Braced Wing in pitch and plunge oscillations. Unsteady lift and pitching moment coefficients are obtained and used to develop the correction terms in the Theodorsen's theory to account for transonic aerodynamics. The unsteady lift and pitching moment derivatives with respect to the unsteady angle of attack are obtained as frequency response functions of the reduced frequency. These frequency response functions are used to compute the dynamic stability derivatives of lift and pitching moment due to the angle of attack and pitch rate and the dynamic stability derivatives for the rolling moment and yawing moment with respect to the roll rate and yaw rate. A transonic correction is applied to steady-state stability derivatives computed by VSPAERO solver using transonic small disturbance code TSFOIL coupled to an integral boundary method. A dynamic stability analysis is conducted for longitudinal and lateral-directional motions. Without transonic corrections and dynamic stability derivatives, the analysis indicates an unstable phugoid mode. The transonic correction applied to the steady-state stability derivatives computed by VSPAERO shows a stable phugoid mode. This is due to the increase of the drag stability derivatives as a result of the additional wave drag contribution in transonic flow. The effect of the transonic dynamic stability derivatives is observed to be a significant contributor to the increase in the damping values of all the flight dynamic modes of the Mach 0.745 Transonic-Truss Braced Wing.

I. Introduction

The Subsonic Ultra Green Aircraft Research (SUGAR) Transonic Truss-Braced Wing (TTBW) aircraft concept is a Boeing-developed N+3 aircraft configuration funded by the NASA ARMD Advanced Air Transport Technologies (AATT) project.[1,2] The TTBW aircraft concept is designed to be aerodynamically efficient by employing a wing aspect ratio of about 19.55 which is significantly greater than those of cantilever wing transport configurations. For example, the latest Boeing 777-X is reported to have a wing aspect ratio of 11. Without structural bracing, the increase in the wing root bending moment would require a significant structural reinforcement which would lead to an increase in the structural weight that would offset the aerodynamic benefit of the high aspect ratio wing. Thus, the design of a truss-braced structure is a multidisciplinary design optimization process that strives to achieve a delicate balance between aerodynamic efficiency and structural efficiency. In the SUGAR configuration, the trade between the aerodynamic performance and structural design results in a truss-braced configuration with the wings braced at approximately mid-span by two main struts. In addition, two jury struts, one on each wing, provide the additional structural reinforcement. Two versions of the TTBW configurations are currently being developed by Boeing; a Mach 0.745 version and a Mach 0.8 version. Figure 1 is an illustration of the Mach 0.745 TTBW aircraft.

*Senior Research Scientist and Technical Group Lead of Advanced Control and Engineering Systems Group, Intelligent Systems Division, nhan.t.nguyen@nasa.gov AIAA Associate Fellow
†Aerospace Engineer, Intelligent System Division, juntao.xiong@nasa.gov

Figure 1. Boeing SUGAR Transonic Truss-Braced Wing Aircraft Concept

This study examines the dynamic stability of the Mach 0.745 TTBW. To analyze dynamic stability of transonic aircraft, capabilities for addressing transonic aerodynamics in the evaluation of both steady-state and dynamic stability derivatives are needed. Toward this end, a transonic correction method has been developed to address this need. A new method for extending the classical Theodorsen's theory[3] of unsteady aerodynamics for incompressible flow to transonic flow is initially proposed by the author.[4–6] Further development has been conducted and leads to the current method.[7] The method modifies the Theodorsen's theory to correct for changes in the amplitude and phase shift of the lift and pitching moment of created by transonic flow over an transonic airfoil in pitch and plunge. The amplitude and phase shift corrections are generally a function of the flow parameters such as the Mach number, the reduced frequency, and the instantaneous angle of attack as well the airfoil characteristics such as the thickness and the type of airfoil. To derive the unsteady corrections, unsteady RANS CFD simulations are performed using FUN3D for selected reduced frequencies and Mach numbers for several transonic airfoil wing sections of the Mach 0.745 TTBW aircraft configuration.[1,2]

The unsteady lift and pitching moment derivatives with respect to the unsteady angle of attack are obtained as frequency response functions over a range of the reduced frequency parameter. The frequency response functions are integrated over the wing to account for the angle of attack, pitch rate, roll rate, and yaw rate contributions. The integrated frequency response functions are then approximated using the Roger rational fraction approximation to obtain the dynamic stability derivatives of lift and pitching moment due to the angle of attack and pitch rate and the dynamic stability derivatives for the rolling moment and yawing moment with respect to the roll rate and yaw rate. The steady-state stability derivatives are computed from VSPAERO solver for inviscid subsonic flow. A transonic correction is applied to steady-state stability derivatives using transonic small disturbance code TSFOIL coupled to an integral boundary method. The flight dynamic equations of motion are then modified to include the transonic corrected steady-state and dynamic stability derivatives. Linearization of the equations of motion is used to extract the eigenvalues of the flight dynamic modes for stability analysis.

II. Transonic Correction Method

The transonic correction method has been developed for both unsteady lift and pitching moment for transonic flow over an airfoil in pitching and plunging motions.[7] The correction functions are obtained from unsteady RANS CFD simulations of several wing sections of the Mach 0.745 TTBW. In the following section, we will summarize the method for the pitching and plunging motions.

A. Pitching Motion

Consider an oscillating airfoil in a pitching motion with a sinusoidal angle of attack at the frequency ω

$$\alpha = \bar{\alpha} + \tilde{\alpha} \tag{1}$$

$$\tilde{\alpha} = \alpha_0 \sin \omega t = \alpha_0 \sin k\tau \tag{2}$$

where $\tau = \frac{2V_\infty t}{c}$ is a non-dimensional time, V_∞ is the freestream airspeed, c is the airfoil chord, and $k = \frac{\omega c}{2V_\infty}$ is the reduced frequency.

1. Unsteady Lift Correction

The unsteady lift coefficient is expressed as

$$c_l = \bar{c}_l + \tilde{c}_l \tag{3}$$

where $\bar{c}_l = c_{l_0} + c_{l_\alpha}\bar{\alpha}$ is the steady-state lift coefficient and $\tilde{c}_l$ is the unsteady lift coefficient.

The unsteady transonic correction to the unsteady lift coefficient is proposed as

$$\tilde{c}_l = (U_\alpha + iW_\alpha)\frac{c_{l_\alpha}}{c_{l_\alpha^*}}\tilde{c}_l^* \tag{4}$$

where $U_\alpha(k, M_\infty, \bar{\alpha}, \alpha_0)$ and $W_\alpha(k, M_\infty, \bar{\alpha}, \alpha_0)$ are transonic correction functions to be applied to the Theodorsen's unsteady lift coefficient, denoted by $\tilde{c}_l^*$, of an oscillating airfoil in incompressible flow, $c_{l_\alpha}^* = 2\pi$, and c_{l_α} is the steady-state lift curve slope. The complex-valued correction provides both the amplitude and phase corrections to the unsteady lift by the functions $U_\alpha(k, M_\infty, \bar{\alpha}, \alpha_0)$ and $W_\alpha(k, M_\infty, \bar{\alpha}, \alpha_0)$, respectively. These functions depend on the reduced frequency k, Mach number M_∞, the mean angle of attack $\bar{\alpha}$, the amplitude of the alternating component of the angle of attack α_0.

The unsteady lift coefficient $\tilde{c}_l^*$ is established by the Theodorsen's theory as

$$\tilde{c}_l^* = c_{l_c}^* + c_{l_{nc}}^* \tag{5}$$

where $c_{l_c}^*$ is the circulatory lift coefficient and $c_{l_{nc}}^*$ is the noncirculatory lift coefficient established by the Theodorsen's theory.

The circulatory lift coefficient $c_{l_c}^*$ is given by

$$c_{l_c}^* = C(k)\, c_{l_\alpha}^* \left(\tilde{\alpha} + 2\frac{e_c}{c}\frac{c\dot{\alpha}}{2V_\infty}\right) = [F(k) + iG(k)]\, c_{l_\alpha}^* \left(\tilde{\alpha} + 2\frac{e_c}{c}\frac{d\alpha}{d\tau}\right) \tag{6}$$

For a harmonic motion with $\theta = e^{ik\tau}$, we have $\frac{d\theta}{d\tau} = ik\theta$ and $\frac{d^2\theta}{d\tau^2} = ik\frac{d\theta}{d\tau} = -k^2\theta$. Then,

$$c_{l_c}^* = \left[F(k) - 2k\frac{e_c}{c}G(k)\right] c_{l_\alpha}^* \alpha_0 \sin k\tau + \left[G(k) + 2k\frac{e_c}{c}F(k)\right] c_{l_\alpha}^* \alpha_0 \cos k\tau \tag{7}$$

The noncirculatory lift coefficient $c_{l_{nc}}^*$ is due to the inertial force acting on the oscillating airfoil and is given by

$$c_{l_{nc}}^* = \pi\frac{c\dot{\alpha}}{2V_\infty} + 2\pi\frac{e_m}{c}\frac{c^2\ddot{\alpha}}{4V_\infty^2} = \pi\frac{d\alpha}{d\tau} + 2\pi\frac{e_m}{c}\frac{d^2\alpha}{d\tau^2} = \pi k\alpha_0\left(\cos k\tau - 2k\frac{e_m}{c}\sin k\tau\right) \tag{8}$$

The unsteady lift coefficient $\tilde{c}_l^*$ is obtained as

$$\tilde{c}_l^* = c_{l_\alpha}^* \alpha_0 (F_k \sin k\tau + G_k \cos k\tau) \tag{9}$$

where

$$F_k = F(k) - 2k\frac{e_c}{c}G(k) - k^2\frac{e_m}{c} \tag{10}$$

$$G_k = G(k) + 2k\frac{e_c}{c}F(k) + \frac{k}{2} \tag{11}$$

The unsteady lift coefficient with the transonic correction is evaluated by

$$\tilde{c}_l = F_k c_{l_\alpha} \alpha_0 \left(U_\alpha \sin k\tau + W_\alpha \cos k\tau\right) + G_k c_{l_\alpha} \alpha_0 \left(U_\alpha \cos k\tau - W_\alpha \sin k\tau\right) \tag{12}$$

where the transonic amplitude and phase lift correction functions U and W are obtained from the Fourier sine and cosine transforms of the unsteady lift coefficient as

$$U_\alpha = \frac{k\left(F_k \int_0^{\frac{2n\pi}{k}} \tilde{c}_l \sin k\tau d\tau + G_k \int_0^{\frac{2n\pi}{k}} \tilde{c}_l \cos k\tau d\tau\right)}{n\pi\left(F_k^2 + G_k^2\right) c_{l_\alpha} \alpha_0} \tag{13}$$

$$W_\alpha = \frac{k\left(F_k \int_0^{\frac{2n\pi}{k}} \tilde{c}_l \cos k\tau d\tau - G_k \int_0^{\frac{2n\pi}{k}} \tilde{c}_l \sin k\tau d\tau\right)}{n\pi\left(F_k^2 + G_k^2\right) c_{l_\alpha} \alpha_0} \tag{14}$$

with n being the number of periods of oscillation.

2. *Unsteady Pitching Moment Correction*

For incompressible flow, the aerodynamic center is at the quarter-chord point. For supersonic flow, the aerodynamic center moves to the mid-chord point. Thus, for transonic flow, the aerodynamic center moves between the quarter-chord and mid-chord points due to the moving shock structure. The motion of the aerodynamic center may be modeled as

$$x_{ac} = \bar{x}_{ac} + x_0 \sin\left(\omega t - \phi\right) = \bar{x}_{ac} + x_0 \sin\left(k\tau - \phi\right) \tag{15}$$

where ϕ is the phase delay angle between the angle of attack motion and the aerodynamic center motion. We make an assumption that the unsteady motion of the aerodynamic center is proportional to the unsteady angle of attack such that

$$\frac{x_{ac}}{c} = \frac{\bar{x}_{ac}}{c} + \left(A_\alpha + iB_\alpha\right) \frac{\tilde{\alpha}}{\alpha_0} \tag{16}$$

where the functions $A_\alpha\left(k, M_\infty, \bar{\alpha}, \alpha_0\right)$ and $B_\alpha\left(k, M_\infty, \bar{\alpha}, \alpha_0\right)$ represent the amplitude and phase angle of the motion of the aerodynamic center.

The steady-state pitching moment coefficient about the pitch center can be expressed as

$$\bar{c}_m = c_{m_{ac}} + \frac{\bar{e}}{c} \bar{c}_l \tag{17}$$

where $\bar{e} = x_e - \bar{x}_{ac}$ is the distance between the pitch center and mean aerodynamic center.

From the steady-state aerodynamics, we obtain

$$\frac{\partial \bar{c}_m}{\partial \bar{\alpha}} = \frac{\partial c_{m_{ac}}}{\partial \bar{\alpha}} + \frac{\bar{e}}{c} c_{l_\alpha} \tag{18}$$

By the definition of an aerodynamic center, $\frac{\partial c_{m_{ac}}}{\partial \bar{\alpha}} = 0$. Therefore, we write

$$\bar{c}_m = \bar{c}_{m_0} + c_{m_\alpha} \bar{\alpha} \tag{19}$$

where $\bar{c}_{m_0} = c_{m_{ac}} + \frac{\bar{e}}{c} \bar{c}_{l_0}$ is the pitching moment coefficient about the pitch center at the zero angle of attack and c_{m_α} is the pitching moment curve slope about the pitch center.

Using the pitching moment curve slope c_{m_α}, the distance $\bar{e}$ between the pitch center and mean aerodynamic center can be determined as

$$\frac{\bar{e}}{c} = \frac{c_{m_\alpha}}{c_{l_\alpha}} \tag{20}$$

Then, the pitching moment coefficient about the aerodynamic center is obtained as

$$c_{m_{ac}} = \bar{c}_m - \frac{c_{m_\alpha}}{c_{l_\alpha}} \bar{c}_l \tag{21}$$

The circulatory pitching moment coefficient about the pitch center is given by

$$c_{m_c} = \left[\frac{\bar{e}}{c} - (A_\alpha + iB_\alpha)\frac{\tilde{\alpha}}{\alpha_0}\right] c_{l_c} - (A_\alpha + iB_\alpha)\frac{\tilde{\alpha}}{\alpha_0}\bar{c}_l \tag{22}$$

The circulatory lift coefficient is computed as

$$\begin{aligned} c_{l_c} = &\left[F(k) - 2k\frac{e_c}{c}G(k)\right] c_{l_\alpha}\alpha_0 (U\sin k\tau + W\cos k\tau) \\ &+ \left[G(k) + 2k\frac{e_c}{c}F(k)\right] c_{l_\alpha}\alpha_0 (U\cos k\tau - W\sin k\tau) \end{aligned} \tag{23}$$

Then, the circulatory pitching moment coefficient about the pitch center is obtained as

$$\begin{aligned} c_{m_c} = &\left(\frac{\bar{e}}{c}F_c - \bar{c}_l A_\alpha\right)\sin k\tau + \left(\frac{\bar{e}}{c}G_c - \bar{c}_l B_\alpha\right)\cos k\tau \\ &- \frac{1}{2}(F_c A_\alpha - G_c B_\alpha) + \frac{1}{2}(F_c A_\alpha - G_c B_\alpha)\cos 2k\tau - \frac{1}{2}(G_c A_\alpha + F_c B_\alpha)\sin 2k\tau \end{aligned} \tag{24}$$

where

$$F_c = \left[F(k) - 2k\frac{e_c}{c}G(k)\right] c_{l_\alpha}\alpha_0 U_\alpha - \left[G(k) + 2k\frac{e_c}{c}F(k)\right] c_{l_\alpha}\alpha_0 W_\alpha \tag{25}$$

$$G_c = \left[G(k) + 2k\frac{e_c}{c}F(k)\right] c_{l_\alpha}\alpha_0 U_\alpha + \left[F(k) - 2k\frac{e_c}{c}G(k)\right] c_{l_\alpha}\alpha_0 W_\alpha \tag{26}$$

In addition, a transonic correction for the noncirculatory pitching moment coefficient is proposed as

$$c_{m_{nc}} = (T_\alpha + iV_\alpha)\, c^*_{m_{nc}} \tag{27}$$

where $c^*_{m_{nc}}$ is the incompressible noncirculatory pitching moment given by the Theodorsen's theory as

$$c^*_{m_{nc}} = \pi\alpha_0 k\left[\frac{k}{16}\left(1 + 32\frac{e_m^2}{c^2}\right)\sin k\tau - \frac{e_c}{c}\cos k\tau\right] \tag{28}$$

Thus, the total unsteady pitching moment coefficient is expressed as

$$\tilde{c}_m = \left[\frac{\bar{e}}{c} - (A_\alpha + iB_\alpha)\frac{\tilde{\alpha}}{\alpha_0}\right] c_{l_c} - (A_\alpha + iB_\alpha)\frac{\tilde{\alpha}}{\alpha_0}\bar{c}_l + (T_\alpha + iV_\alpha)\, c^*_{m_{nc}} \tag{29}$$

Summing all the contributions of the pitching moment coefficient, the unsteady pitching moment coefficient is obtained as

$$\tilde{c}_m = F_m\sin k\tau + G_m\cos k\tau - \frac{1}{2}(G_c A_\alpha + F_c B_\alpha)\sin 2k\tau + \frac{1}{2}(F_c A_\alpha - G_c B_\alpha)\cos 2k\tau \tag{30}$$

where

$$F_m = \frac{\bar{e}}{c}F_c - \bar{c}_l A_\alpha + \pi\alpha_0 k\left[\frac{k}{16}\left(1 + 32\frac{e_m^2}{c^2}\right)T_\alpha + \frac{e_c}{c}V_\alpha\right] \tag{31}$$

$$G_m = \frac{\bar{e}}{c}G_c - \bar{c}_l B_\alpha + \pi\alpha_0 k\left[\frac{k}{16}\left(1 + 32\frac{e_m^2}{c^2}\right)V_\alpha - \frac{e_c}{c}T_\alpha\right] \tag{32}$$

Thus, the transonic pitching moment correction functions A_α, B_α, T_α, and V_α are obtained from the Fourier sine and cosine transforms of the unsteady pitching moment coefficients as

$$A_\alpha = \frac{2k\left(F_c\int_0^{\frac{2n\pi}{k}}\tilde{c}_m\cos 2k\tau d\tau - G_c\int_0^{\frac{2n\pi}{k}}\tilde{c}_m\sin 2k\tau d\tau\right)}{n\pi(F_c^2 + G_c^2)} \tag{33}$$

$$B_\alpha = -\frac{2k\left(F_c\int_0^{\frac{2n\pi}{k}}\tilde{c}_m\sin 2k\tau d\tau + G_c\int_0^{\frac{2n\pi}{k}}\tilde{c}_m\cos 2k\tau d\tau\right)}{n\pi(F_c^2 + G_c^2)} \tag{34}$$

$$T_\alpha = \frac{\frac{k}{16}\left(1+32\frac{e_m^2}{c^2}\right)\left(F_m - \frac{\bar{e}}{c}F_c + \bar{c}_l A_\alpha\right) - \frac{e_c}{c}\left(G_m - \frac{\bar{e}}{c}G_c + \bar{c}_l B_\alpha\right)}{\pi\alpha_0 k\left[\left(\frac{k}{16}\right)^2\left(1+32\frac{e_m^2}{c^2}\right)^2 + \left(\frac{e_c}{c}\right)^2\right]} \tag{35}$$

$$V_\alpha = \frac{\frac{k}{16}\left(1+32\frac{e_m^2}{c^2}\right)\left(G_m - \frac{\bar{e}}{c}G_c + \bar{c}_l B_\alpha\right) + \frac{e_c}{c}\left(F_m - \frac{\bar{e}}{c}F_c + \bar{c}_l A_\alpha\right)}{\pi\alpha_0 k\left[\left(\frac{k}{16}\right)^2\left(1+32\frac{e_m^2}{c^2}\right)^2 + \left(\frac{e_c}{c}\right)^2\right]} \tag{36}$$

B. Plunging Motion

The motion of an airfoil in plunge is related to the pitching motion by the effective angle of attack

$$\tilde{\alpha} = \frac{\dot{h}}{V_\infty} \tag{37}$$

The plunging motion is described by

$$h = -h_0 \cos\omega t = -h_0 \cos k\tau \tag{38}$$

Then, the airfoil sees an angle of attack

$$\alpha = \bar{\alpha} + \frac{\dot{h}}{V_\infty} = \bar{\alpha} + \frac{2h_0 k}{c}\sin k\tau \tag{39}$$

To establish the equivalent angle of attack, the plunging motion is prescribed by setting $\alpha_0 = \frac{2h_0 k}{c}$.

1. Unsteady Lift Correction

Applying the transonic correction, the unsteady lift coefficient for the plunging motion are expressed as

$$\begin{aligned}\tilde{c}_l &= (U_h + iW_h)\, c_{l_\alpha}\left[C(k)\frac{2}{c}\frac{dh}{d\tau} + \frac{1}{c}\frac{d^2h}{d\tau^2}\right] \\ &= c_{l_\alpha}\alpha_0\left[FU_h - \left(G+\frac{k}{2}\right)W_h\right]\sin k\tau + c_{l_\alpha}\alpha_0\left[\left(G+\frac{k}{2}\right)U_h + FW_h\right]\cos k\tau\end{aligned} \tag{40}$$

Thus, the correction functions U_h and W_h are obtained from the Fourier sine and cosine transforms of the unsteady lift coefficient as

$$U_h = \frac{k\left[F\int_0^{\frac{2n\pi}{k}}\tilde{c}_l \sin k\tau d\tau + \left(G+\frac{k}{2}\right)\int_0^{\frac{2n\pi}{k}}\tilde{c}_l \cos k\tau d\tau\right]}{n\pi c_{l_\alpha}\alpha_0\left[F^2 + \left(G+\frac{k}{2}\right)^2\right]} \tag{41}$$

$$W_h = \frac{k\left[F_k\int_0^{\frac{2n\pi}{k}}\tilde{c}_l \cos k\tau d\tau - \left(G+\frac{k}{2}\right)\int_0^{\frac{2n\pi}{k}}\tilde{c}_l \sin k\tau d\tau\right]}{n\pi c_{l_\alpha}\alpha_0\left[F^2 + \left(G+\frac{k}{2}\right)^2\right]} \tag{42}$$

2. Unsteady Pitching Moment Correction

The unsteady pitching moment coefficient for the plunging motion can be corrected as

$$\tilde{c}_m = \left[\frac{\bar{e}}{c} - (A_h + iB_h)\frac{1}{h_0 k}\frac{dh}{d\tau}\right](U_h + iW_h)\, c_{l_\alpha} C(k)\frac{2}{c}\frac{dh}{d\tau} - (T_h + iV_h)\, 2\pi\frac{e_m}{c}\frac{1}{c}\frac{d^2h}{d\tau^2} \tag{43}$$

The expression for the unsteady pitching moment coefficient is expanded as

$$\tilde{c}_m = \left(\frac{\bar{e}}{c}F_h + \pi k\alpha_0 \frac{e_m}{c}V_h\right)\sin k\tau + \left(\frac{\bar{e}}{c}G_h - \pi k\alpha_0 \frac{e_m}{c}T_h\right)\cos k\tau$$
$$-\frac{1}{2}\left(F_h A_h - G_h B_h\right) + \frac{1}{2}\left(F_h A_h - G_h B_h\right)\cos 2k\tau - \frac{1}{2}\left(G_h A_h + F_h B_h\right)\sin 2k\tau \tag{44}$$

where

$$F_h = c_{l_\alpha}\alpha_0\left(FU_h - GW_h\right) \tag{45}$$

$$G_h = c_{l_\alpha}\alpha_0\left(GU_h + FW_h\right) \tag{46}$$

Thus, we obtain the transonic correction functions A_h, B_h, T_h, and V_h from the Fourier sine and cosine transforms of the unsteady pitching coefficient as

$$A_h = \frac{2k\left(F_h\int_0^{\frac{2n\pi}{k}}\tilde{c}_m\cos 2k\tau d\tau - G_h\int_0^{\frac{2n\pi}{k}}\tilde{c}_m\sin 2k\tau d\tau\right)}{n\pi\left(F_h^2+G_h^2\right)} \tag{47}$$

$$B_h = -\frac{2k\left(F_h\int_0^{\frac{2n\pi}{k}}\tilde{c}_m\sin 2k\tau d\tau + G_h\int_0^{\frac{2n\pi}{k}}\tilde{c}_m\cos 2k\tau d\tau\right)}{n\pi\left(F_h^2+G_h^2\right)} \tag{48}$$

$$T_h = \frac{-\frac{k}{n\pi}\int_0^{\frac{2n\pi}{k}}\tilde{c}_m\cos k\tau d\tau + \frac{\bar{e}}{c}G_h}{\pi k\alpha_0\frac{e_m}{c}} \tag{49}$$

$$V_h = \frac{\frac{k}{n\pi}\int_0^{\frac{2n\pi}{k}}\tilde{c}_m\sin k\tau d\tau - \frac{\bar{e}}{c}F_h}{\pi k\alpha_0\frac{e_m}{c}} \tag{50}$$

III. Application of Transonic Correction in Unsteady Flow Simulations

A series of unsteady RANS CFD simulations of oscillating transonic airfoils are conducted in FUN3D. The airfoils are extracted from the Boeing Mach 0.745 TTBW aircraft configuration at four wing stations as shown in Figure 2. The pitch center of the oscillating airfoils is at the quarter-chord location. The FUN3D mesh has about 30 thousand grid points. The mesh domain size is about 100 times the airfoil chord length. The Roe's flux-difference splitting scheme and the Spalart-Allmaras turbulence model are used in the simulations. An optimized second-order backward finite-difference scheme is used in the time integration. The simulations are conducted in FUN3D for Mach 0.65, 0.7, 0.75, and 0.8 at four different reduced frequencies $k = 0.02$, 0.1, 0.2, and $k = 0.3$.

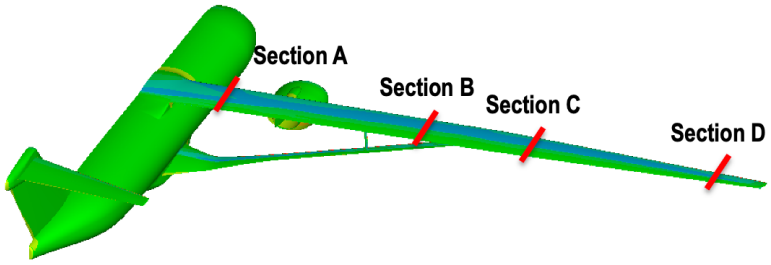

Figure 2. Mach 0.745 Transonic Truss Braced-Wing Airfoil Cuts

Steady-state RANS CFD simulations of the full Mach 0.745 TTBW configuration are also conducted in FUN3D. The Roe's flux-difference splitting scheme and the Spallart-Allmaras turbulence model are used in the simulations. The Venkatakrishnan limiter is also used. The tetrahedral and prism mesh has 90.4 million grid points. The steady state simulations are conducted at Mach 0.65, 0.7, and 0.75. The plots of the section lift coefficients for these wing

sections are shown in Figures 3(a)-(d). From this data set, the trim angles of attack for the wing sections are obtained for the design lift coefficient of 0.73 at Mach 0.745. The wing sweep correction is also applied for each wing station.

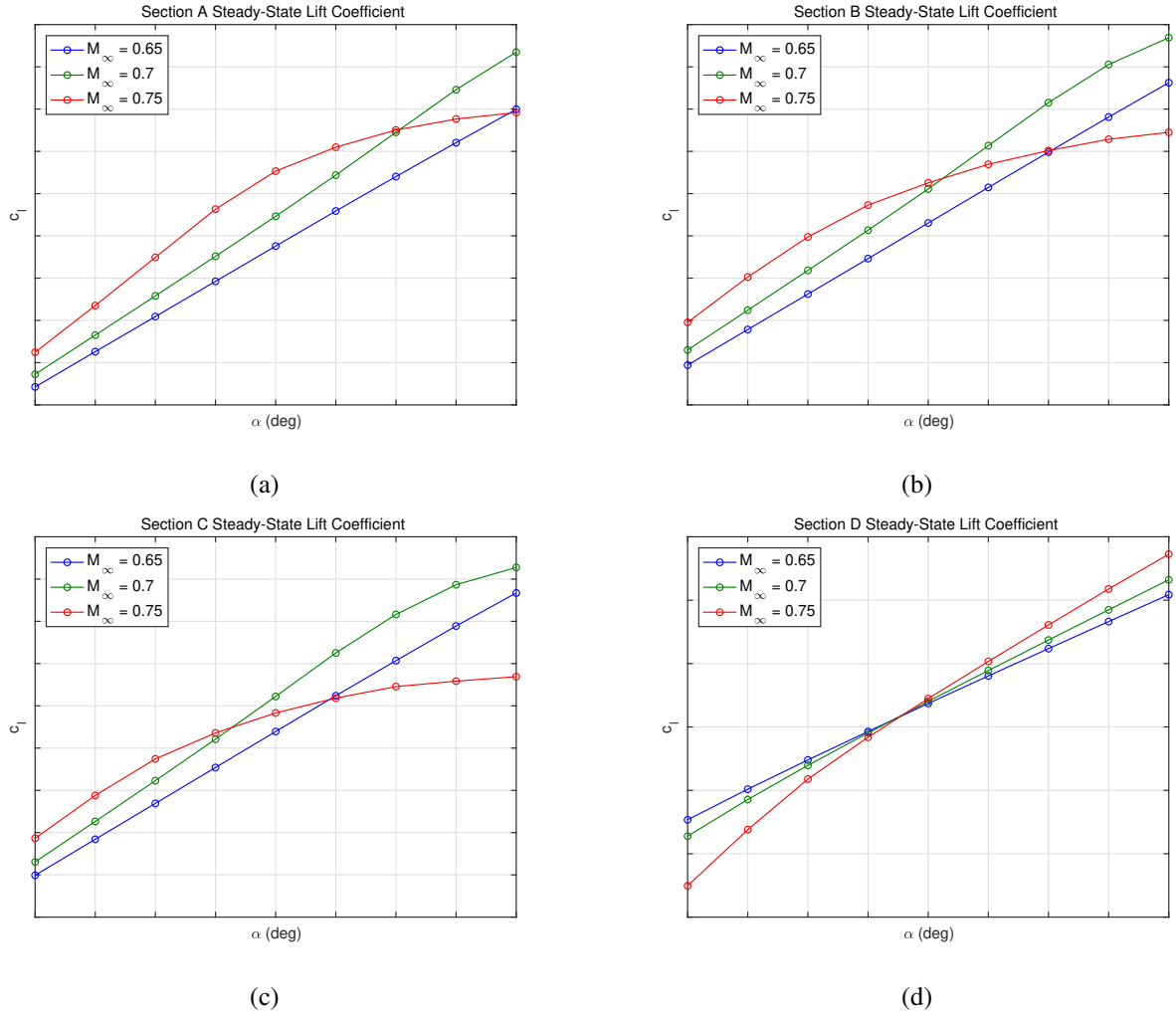

Figure 3. Mach 0.745 Transonic Truss-Braced Wing Section $\bar{c}_l$

Selected figures from the analysis are presented to illustrate the method. Figures 4 (a) and (b) show the time history of the unsteady lift coefficient and the hysteresis loop in the lift curve, respectively, computed by FUN3D for the MAC wing section at Mach 0.8 and the reduced frequency $k = 0.02$. The computed unsteady lift coefficient by the transonic correction method is in good agreement with the FUN3D results.

Figures 5(a) and (b) present the time history of the unsteady pitching moment coefficient and the hysteresis loop in the pitching moment curve, respectively, for Mach 0.8 and the reduced frequency $k = 0.02$. The unsteady pitching moment coefficient exhibits a strong nonlinearity not seen in the unsteady lift coefficient in Figures 4(a) and (b). The transonic correction method is able to capture the nonlinear pitching moment coefficient quite accurately. There is an excellent agreement in the time histories of the unsteady pitching moment coefficients between the FUN3D results and the transonic correction. The hysteresis loop in the pitching moment curve illustrates the strong nonlinearity. The match in the hysteresis loop is generally quite good.

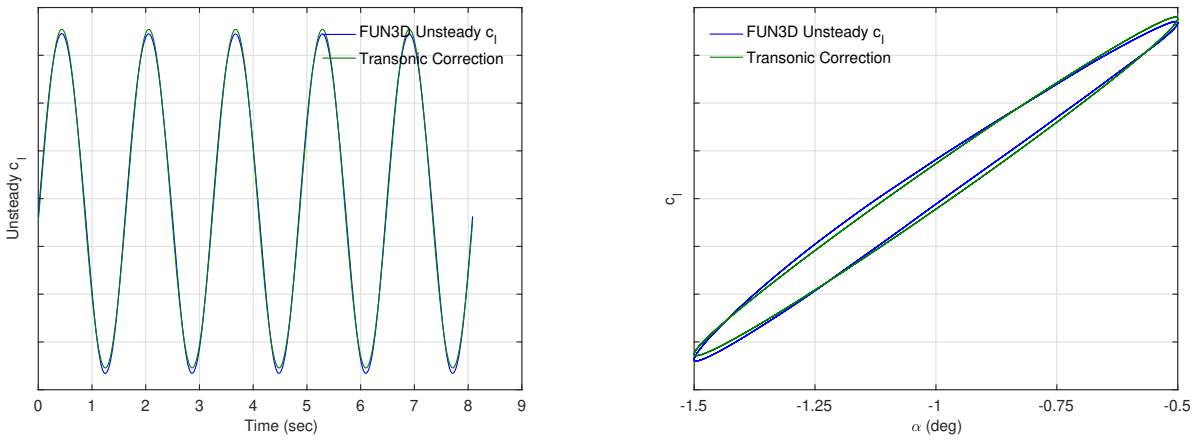

(a) (b)

Figure 4. Mach 0.745 Transonic Truss-Braced Wing MAC Wing Section c_l Time History and c_l vs. α for Mach 0.8 and $k = 0.02$

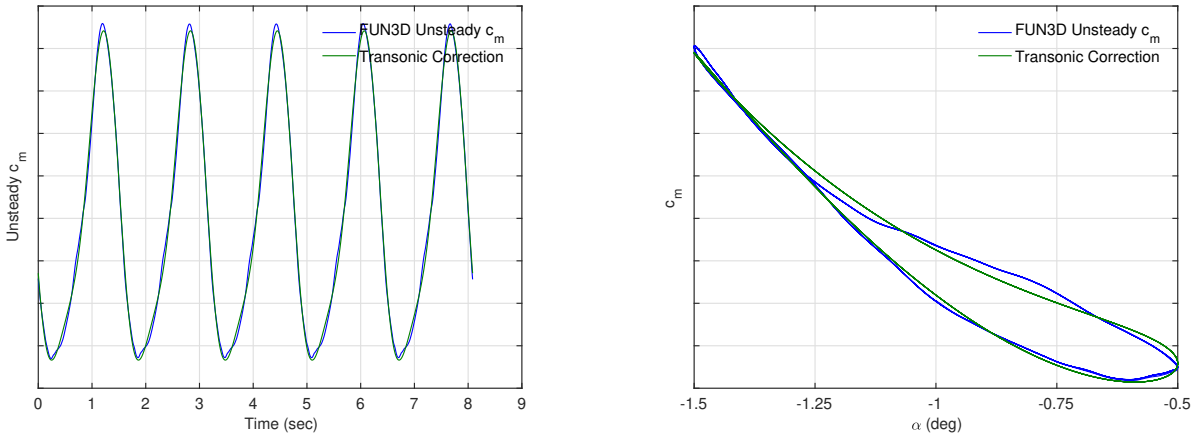

(a) (b)

Figure 5. Mach 0.745 Transonic Truss-Braced Wing MAC Wing Section c_m Time History and c_m vs. α for Mach 0.8 and $k = 0.02$

The nonlinear effect in the unsteady pitching moment coefficient is postulated to be due to the unsteady motion of the aerodynamic center due to the moving shock. This has been confirmed by the shock locations in the previous study.[7] The inclusion of a transonic correction term to capture the unsteady motion of the aerodynamic center allows the transonic correction method to accurately model the unsteady pitching moment coefficient. Figures 6(a) and (b) present the time history of the motion of the aerodynamic center about the mean aerodynamic center and the hysteresis of the aerodynamic center location vs. angle of attack, respectively, computed by the transonic correction method. The motion is predicted to be about 2.3% of chord.

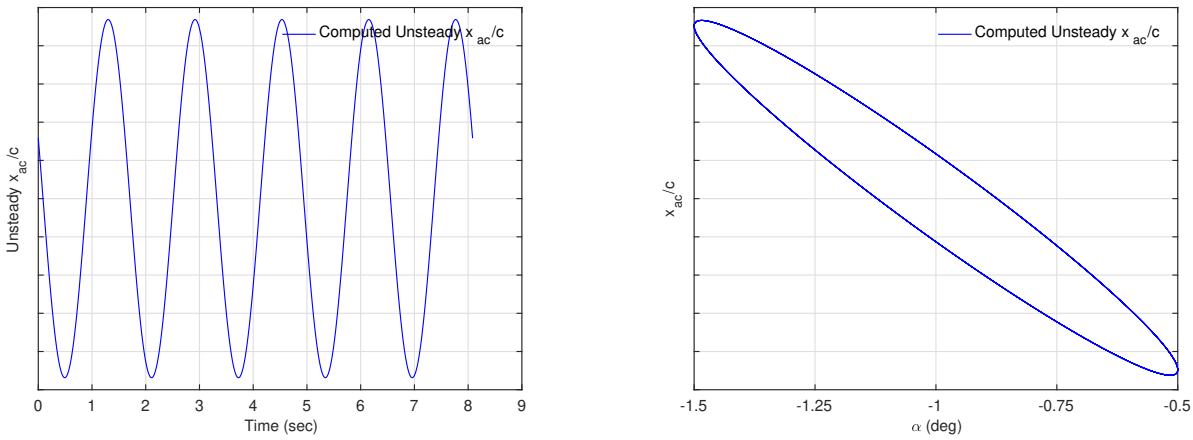

(a) (b)

Figure 6. Mach 0.745 Transonic Truss-Braced Wing MAC Wing Section x_{ac} Time History and x_{ac} vs. α for Mach 0.8 and $k = 0.02$

To illustrate the effect of the reduced frequency, Figures 7(a) and (b) present the time history of the unsteady lift coefficient and the hysteresis loop of the lift curve, respectively, for Mach 0.8 and the reduced frequency $k = 0.3$. The transonic correction method captures the unsteady lift coefficient very accurately.

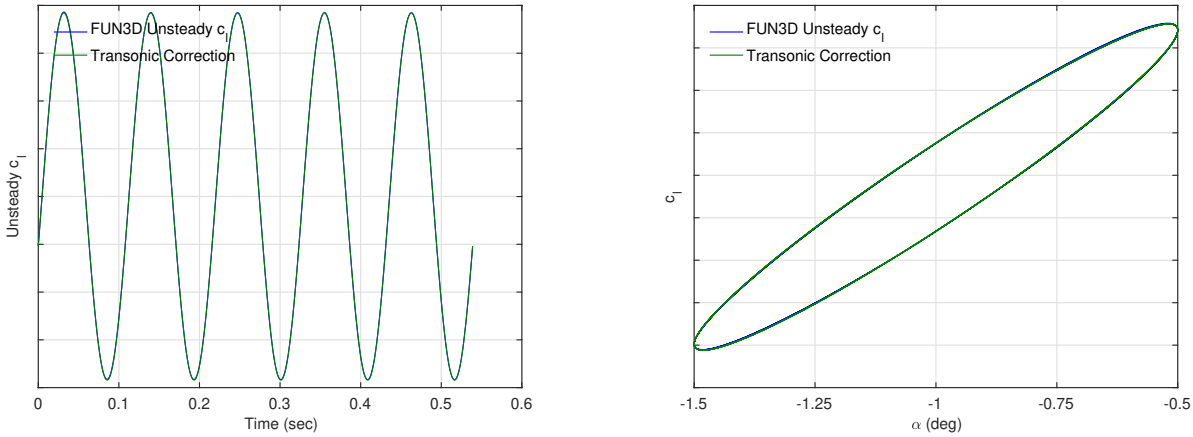

(a) (b)

Figure 7. Mach 0.745 Transonic Truss-Braced Wing MAC Wing Section c_l Time History and c_l vs. α for Mach 0.8 and $k = 0.3$

Figures 8(a) and (b) show the time history of the unsteady pitching moment coefficient and the hysteresis loop of the pitching moment curve, respectively, for Mach 0.8 and the reduced frequency $k = 0.3$. It is interesting to note that the strong nonlinear effect in the unsteady pitching moment coefficient for the reduced frequency $k = 0.02$ is not present in the unsteady pitching moment for the reduced frequency $k = 0.3$. Nonetheless, the hysteresis loop in the unsteady pitching moment curve indicates a slight nonlinearity in the unsteady pitching moment coefficient.

Figures 9(a) and (b) show the time history of the unsteady motion of the aerodynamic center computed by the transonic correction method. It is interesting to see that the amplitude of the motion of the aerodynamic center decreases as the reduced frequency increases when comparing the amplitudes for the reduced frequency $k = 0.02$ in Figures 6 (a) and (b). Moreover, the phase angle of the motion of the aerodynamic center also reverses. A possible explanation for the reduced nonlinearity in the unsteady pitching moment coefficient as the reduced frequency increases could be due to the lift circulation not being able to fully establish at higher values of the reduced frequency. At very small values of the reduced frequency, the flow is dominated by the steady-state lift circulation which is strongly nonlinear

in transonic flow. Therefore, as the flow begins to transition from a steady flow to unsteady flow, the nonlinear effect of the steady flow still dominates.

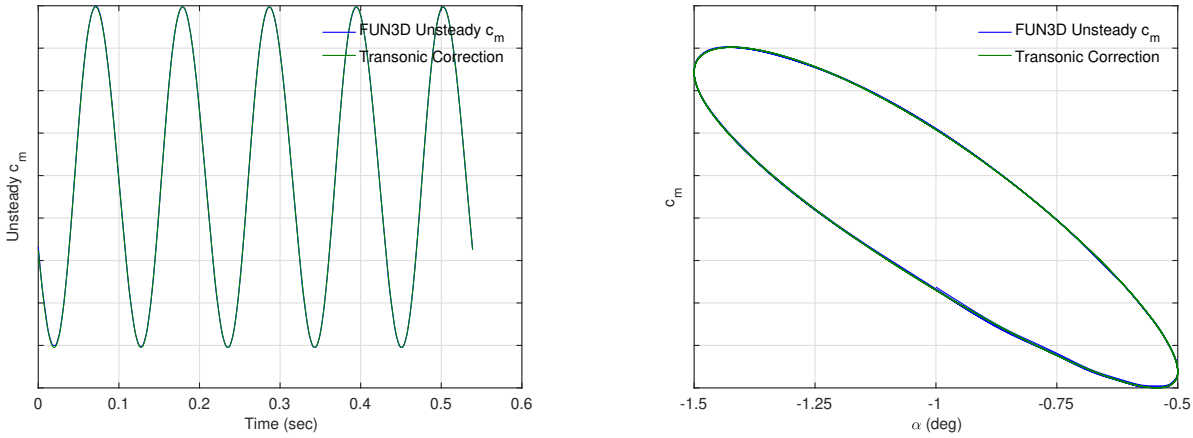

(a) (b)

Figure 8. Mach 0.745 Transonic Truss-Braced Wing MAC Wing Section c_m Time History and c_m vs. α for Mach 0.8 and $k = 0.3$

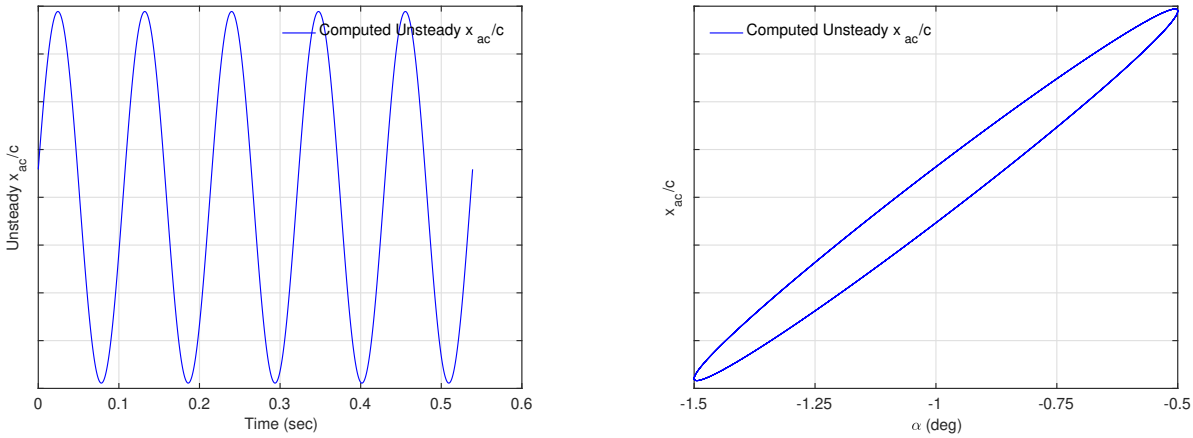

(a) (b)

Figure 9. Mach 0.745 Transonic Truss-Braced Wing MAC Wing Section x_{ac} Time History and x_{ac} vs. α for Mach 0.8 and $k = 0.3$

Figures 10(a) and (b) present the amplitude and phase correction functions U_α and W_α for the unsteady lift coefficient in a pitching harmonic motion, respectively. The functions vary with the Mach number and the reduced frequency for the amplitude of oscillation of 0.5°. The amplitude correction function U_α shows a decrease in the amplitude as the reduced frequency increases at a given Mach number. At the reduced frequency $k = 0.3$, the amplitude decreases by some amount as the Mach number increases from 0.6 to 0.8. The phase correction function W_α also shows an increase in the phase lag as the reduced frequency increases. At the reduced frequency $k = 0.3$, the phase angle decreases as the Mach number increases from 0.6 to 0.8.

Figures 11(a) and (b) present the functions A_α and B_α that model the motion of the aerodynamic center, respectively. The function A_α represents the amplitude of the motion of the aerodynamic center and clearly shows a large amplitude at Mach 0.8 and $k = 0.02$. As the reduced frequency increases, the amplitude of the motion reduces. The function B_α represents the phase angle relative to the motion of the angle of attack. As the reduced frequency increases, the phase angle decreases.

Figures 12 shows the functions T_α and V_α that correct for the amplitude and phase angle of the noncirculatory

pitching moment coefficient. The functions show large negative values at Mach 0.8 and $k = 0.02$ which indicates a larger correction for the noncirculatory pitching moment coefficient due to the nonlinear effect. As the reduced frequency increases, the correction becomes small.

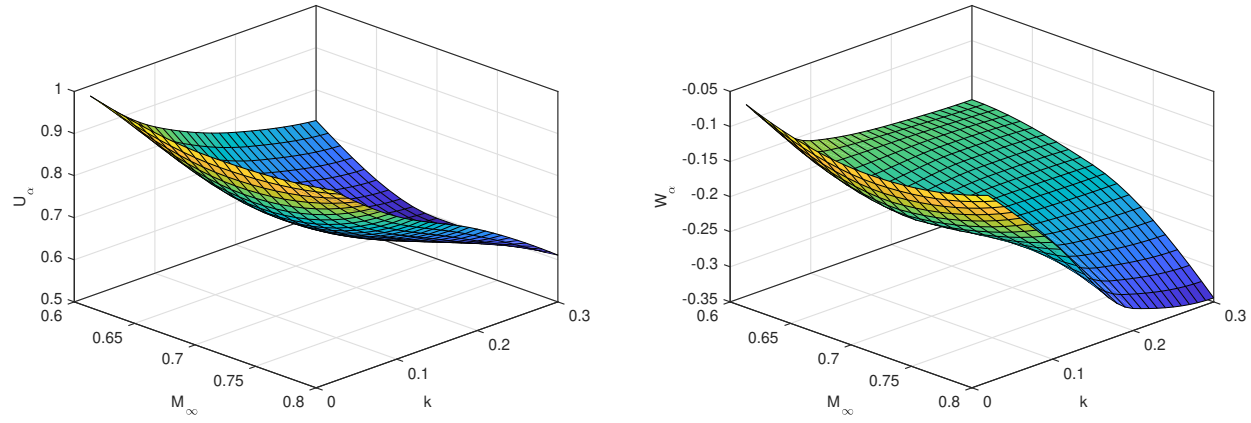

(a) (b)

Figure 10. Mach 0.745 Transonic Truss-Braced Wing MAC Wing Section Transonic Correction Functions U_α and W_α for Unsteady Lift

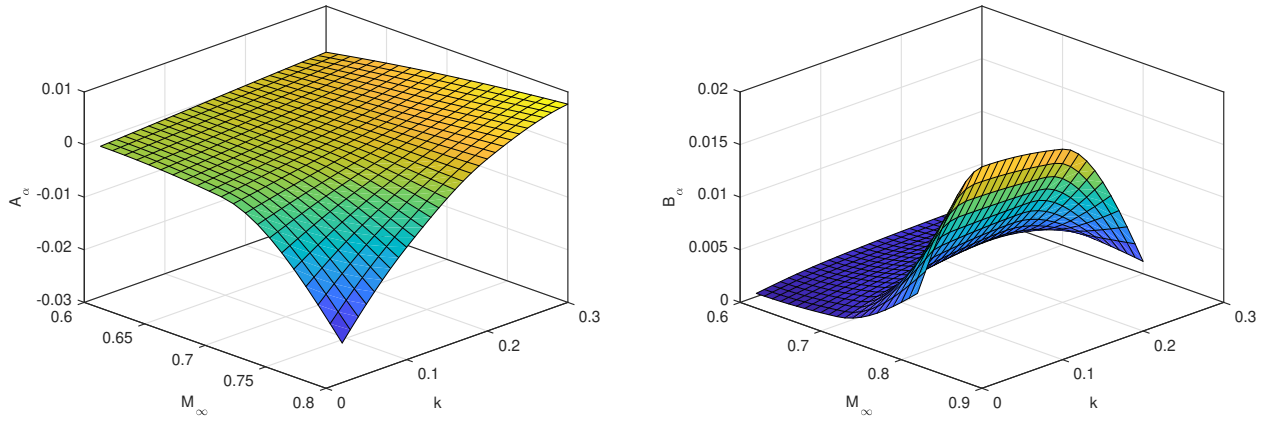

(a) (b)

Figure 11. Mach 0.745 Transonic Truss-Braced Wing MAC Wing Section Transonic Correction Functions A_α and B_α for Aerodynamic Center Motion

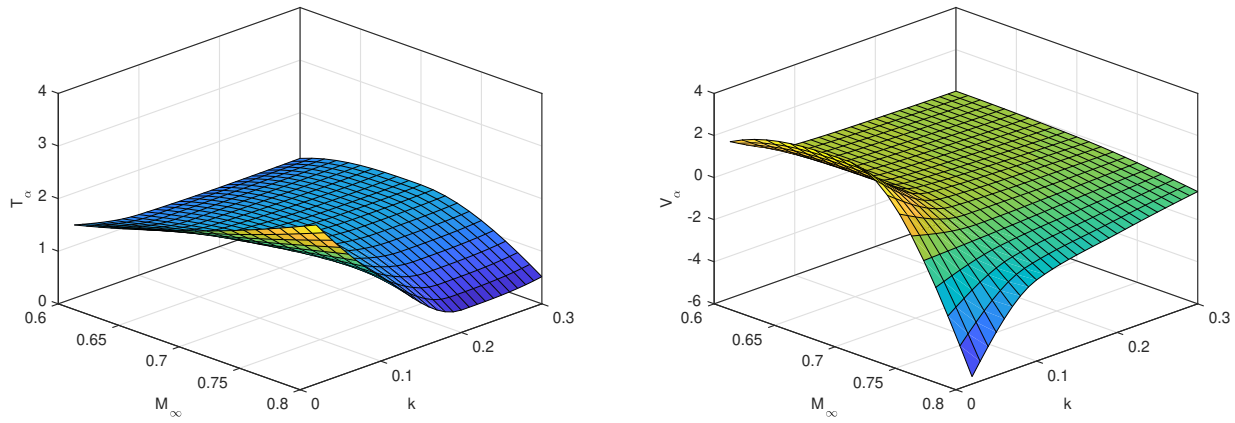

Figure 12. Mach 0.745 Transonic Truss-Braced Wing MAC Wing Section Transonic Correction Functions T_α and V_α for Noncirculatory Pitching Moment

Figures 13(a) and (b) compare the correction functions U_α and W_α for the pitching motion to U_h and W_h for the plunging motion for the unsteady lift as functions of the Mach number, respectively. The amplitude correction U_h for the plunging motion is slightly larger than the amplitude correction function U_α for the pitching motion by an almost constant offset. The phase correction W_h for the plunging motion is smaller in amplitude than the phase correction W_α for the pitching motion. The phase correction greatly increases for Mach 0.75.

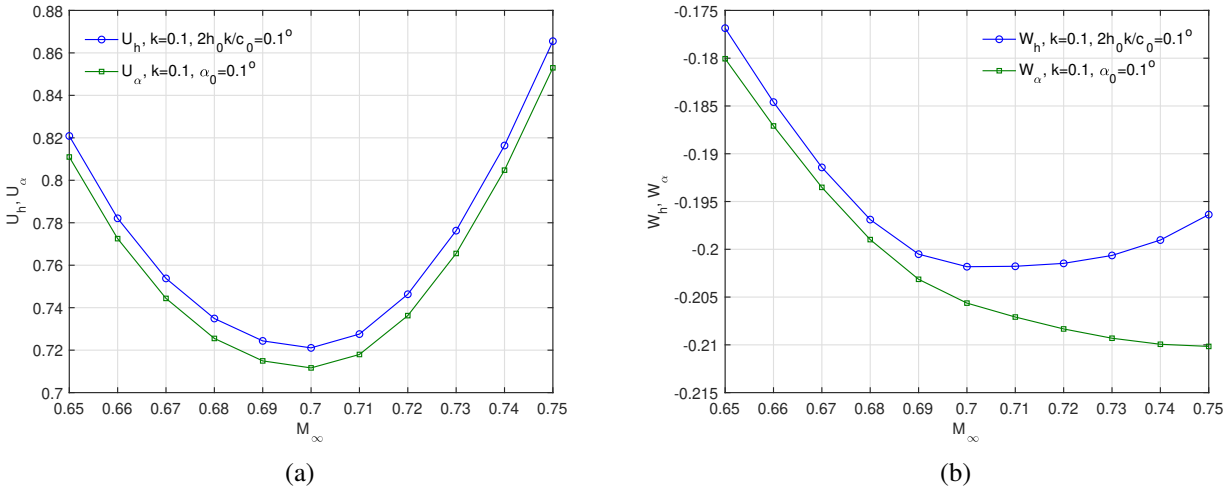

Figure 13. Mach 0.745 Transonic Truss-Braced Wing MAC Airfoil Transonic Correction Functions U_α and W_α for Pitching Motion and U_h and W_h for Plunging Motion for Unsteady Lift versus Mach Number for $k = 0.1$ and $\alpha_0 = \frac{2h_0 k}{c} = 0.1°$

Figures 14(a) and (b) compare the correction functions A_α and B_α for the pitching motion to the correction functions A_h and B_h for the pitching motion for the aerodynamic center motion as functions of the Mach number. These transonic correction functions capture the nonlinearity in the unsteady pitching moment. Their magnitudes generally increase with increasing the Mach number, thereby implying that the flow is increasingly nonlinear as the Mach number increases.

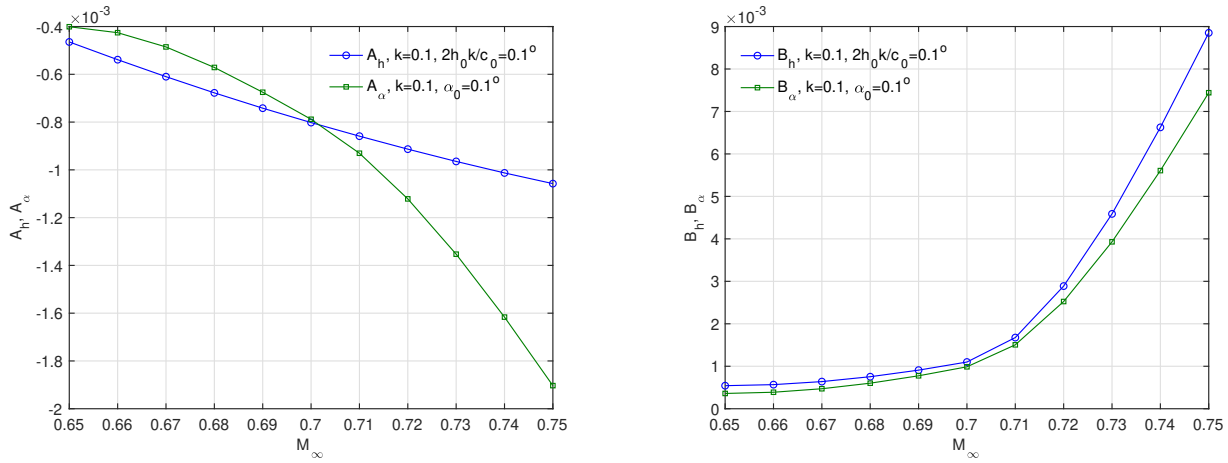

Figure 14. Mach 0.745 Transonic Truss-Braced Wing MAC Airfoil Transonic Correction Functions A_α and B_α for Pitching Motion and A_h and B_h for Plunging Motion for Aerodynamic Center Motion versus Mach Number for $k = 0.1$ and $\alpha_0 = \frac{2h_0 k}{c} = 0.1^\circ$

Figures 15(a) and (b) compare the correction functions T_α and V_α for the pitching motion to the correction functions T_h and V_h for the plunging motion for the noncirculatory pitching moment as functions of the Mach number. The amplitude correction T_α for the pitching motion is larger than amplitude correction T_h for the plunging motion. The phase correction V_α for the pitching motion is slightly smaller in amplitude than the phase correction V_h for the plunging motion.

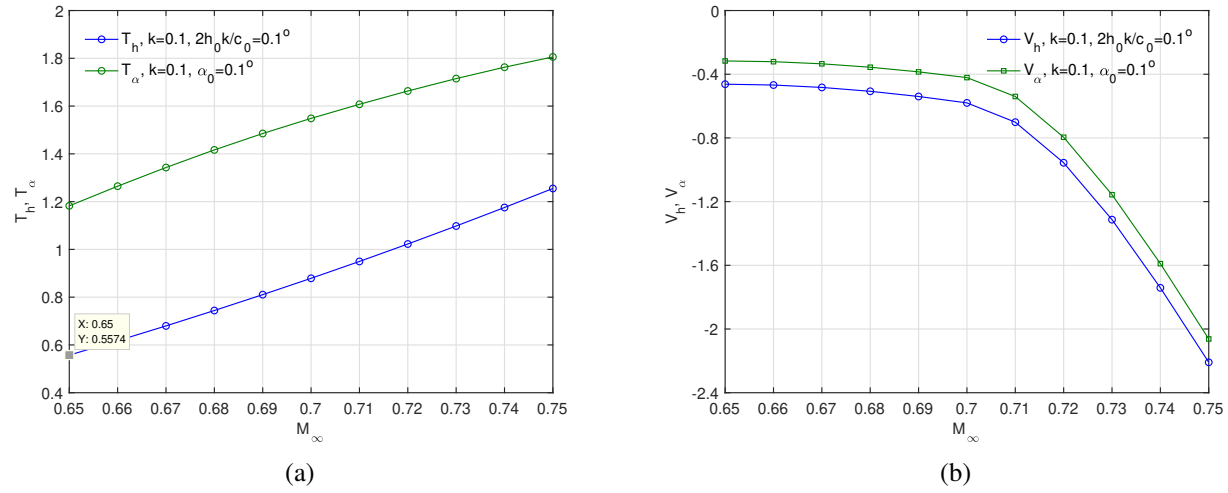

Figure 15. Mach 0.745 Transonic Truss-Braced Wing MAC Airfoil Transonic Correction Functions T_α and V_α for Pitching Motion and T_h and V_h for Plunging Motion for Noncirculatory Pitching Moment versus Mach Number for $k = 0.1$ and $\alpha_0 = \frac{2h_0 k}{c} = 0.1^\circ$

IV. Dynamic Stability Derivative Analysis

From the transonic correction method, we obtain the linear aerodynamic frequency response functions between the unsteady lift and pitching moment coefficients and the oscillating angle of attack $\tilde{\alpha}$ for the pitching motion by neglecting the nonlinear effect of the motion of the aerodynamic center. These linear aerodynamic frequency response

functions for the pitching motion are obtained as

$$c_{l_{\tilde{\alpha}}}(k) = [U_\alpha(k) + iW_\alpha(k)]\, c_{l_\alpha}\left[C(k)\left(1 + 2\frac{e_c}{c}ik\right) + \left(\frac{1}{2}ik - \frac{e_m}{c}k^2\right)\right] \tag{51}$$

$$\begin{aligned} c_{m_{\tilde{\alpha}}}(k) = &\frac{\bar{e}}{c}[U_\alpha(k) + iW_\alpha(k)]\, c_{l_\alpha} C(k)\left(1 + 2\frac{e_c}{c}ik\right) \\ &+ [T_\alpha(k) + iV_\alpha(k)]\left[\pi k^2\left(\frac{1}{16} + 2\frac{e_m^2}{c^2}\right) - i\pi k e_c\right] \end{aligned} \tag{52}$$

The linear aerodynamic frequency response function for the plunging motion are obtained as

$$c_{l_{\hat{h}}}(k) = [U_h(k) + iW_h(k)]\, c_{l_\alpha}\left[C(k) + \frac{1}{2}ik\right] \tag{53}$$

$$c_{m_{\hat{h}}}(k) = \frac{\bar{e}}{c}[U_h(k) + iW_h(k)]\, c_{l_\alpha} C(k) - [T_h(k) + iV_h(k)]\,\pi\frac{e_m}{c}ik \tag{54}$$

where $\hat{\dot{h}} = \frac{\dot{h}}{V_\infty}$.

Figure 16(a) and (b) show the frequency response functions of the dynamic stability derivatives of the MAC wing section lift and pitching moment coefficients with respect to the angle of attack. The frequency response functions are computed by an interpolation of the unsteady CFD simulation data over a reduced frequency range from 0 to 0.2. Figure 17(a) and (b) show the frequency response functions of the dynamic stability derivatives of the MAC wing section lift and pitching moment coefficients with respect to the altitude rate.

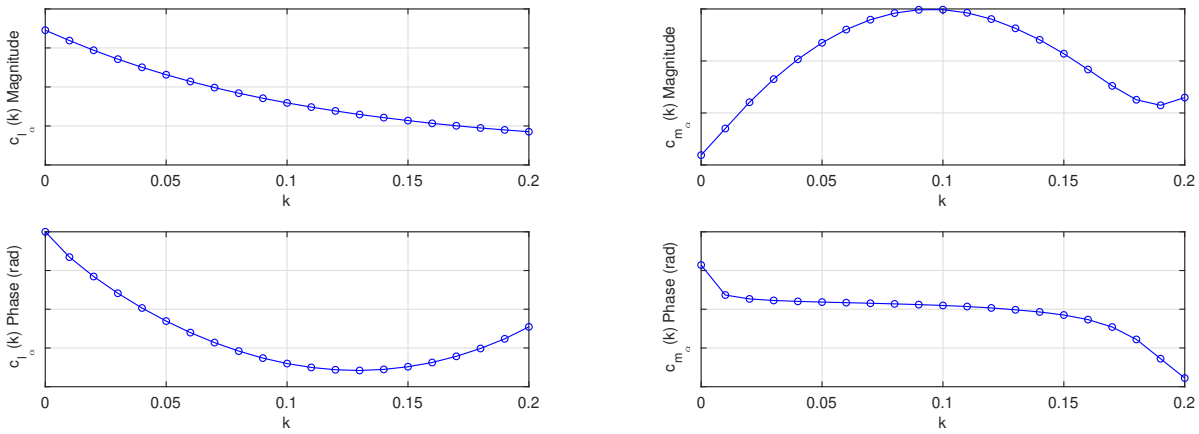

Figure 16. Mach 0.745 Transonic Truss-Braced Wing MAC Wing Section c_{l_α} and $c_{m_{\tilde{\alpha}}}$ Frequency Response Functions

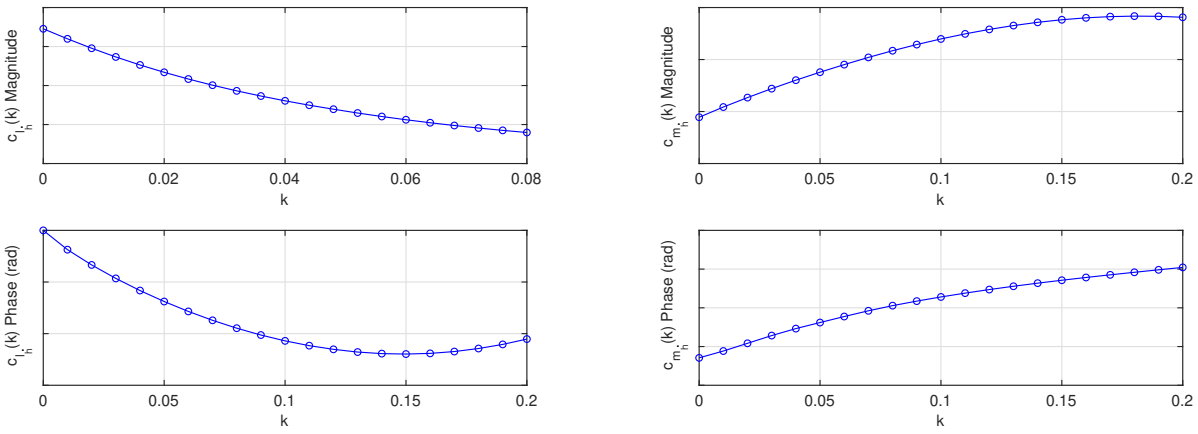

(a) (b)

Figure 17. Mach 0.745 Transonic Truss-Braced Wing MAC Wing Section $c_{l_{\dot{h}}}$ and $c_{m_{\dot{h}}}$ Frequency Response Functions

To obtain the dynamic stability derivatives for the aircraft, the following analyses are performed:

A. Dynamic Stability Derivatives with Respect to Angle of Attack

We assume that the dynamic stability derivatives are dominant by the wing contribution. Furthermore, transonic flow usually is associated with wing aerodynamics due to the high operating lift coefficient in flight. The horizontal tail and vertical tail usually operate at lower lift coefficients. Therefore, the flow is usually subsonic.

The effective center of lift measured from the quarter-chord location is computed as

$$\frac{e}{c} = -\frac{c_{m_{\tilde{\alpha}}}}{c_{l_{\tilde{\alpha}}}} \tag{55}$$

The aircraft lift and pitching moment stability derivatives with respect to the unsteady angle of attack $\tilde{\alpha}$ due to the wing contribution are then obtained as

$$C_{L_{\tilde{\alpha}}} = \frac{1}{S}\int_{\frac{-b}{2}}^{\frac{b}{2}} c_{l_{\tilde{\alpha}}} c\, dy \tag{56}$$

$$C_{m_{\tilde{\alpha}}} = \frac{1}{S\bar{c}}\int_{\frac{-b}{2}}^{\frac{b}{2}} c_{l_{\tilde{\alpha}}}\left(x_{cg} - x_a - e\right) c\, dy = \frac{1}{S\bar{c}}\int_{\frac{-b}{2}}^{\frac{b}{2}} \left[c_{m_{\tilde{\alpha}}} c + c_{l_{\tilde{\alpha}}}\left(x_{cg} - x_a\right)\right] c\, dy \tag{57}$$

where x_{cg} is the aircraft center of gravity (CG) and x_a is wing section at the quarter-chord location.

Similarly, the aircraft lift and pitching moment stability derivatives with respect to the altitude rate $\dot{h}$ due to the wing contribution are obtained as

$$C_{L_{\dot{h}}} = \frac{1}{S}\int_{\frac{-b}{2}}^{\frac{b}{2}} c_{l_{\dot{h}}} c\, dy \tag{58}$$

$$C_{m_{\dot{h}}} = \frac{1}{S\bar{c}}\int_{\frac{-b}{2}}^{\frac{b}{2}} \left[c_{m_{\dot{h}}} c + c_{l_{\dot{h}}}\left(x_{cg} - x_a\right)\right] c\, dy \tag{59}$$

These frequency response functions are then approximated by a rational fraction approximation[8,9] as follows:

$$C_{L_{\tilde{\alpha}}}(\bar{s}) = C_{L_{\ddot{\alpha}}}\bar{s}^2 + C_{L_{\dot{\alpha}}}\bar{s} + C_{L_{\alpha}} + \sum_{i=1}^{6}\frac{a_i \bar{s}}{\bar{s} - p_i} \tag{60}$$

$$C_{m_{\tilde{\alpha}}}(\bar{s}) = C_{m_{\ddot{\alpha}}}\bar{s}^2 + C_{m_{\dot{\alpha}}}\bar{s} + C_{m_{\alpha}} + \sum_{i=1}^{6}\frac{b_i \bar{s}}{\bar{s} - q_i} \tag{61}$$

$$C_{L_{\bar{h}}}(\bar{s}) = C_{L_{\bar{h}}} + \sum_{i=1}^{6} \frac{f_i}{\bar{s} - u_i} \tag{62}$$

$$C_{m_{\bar{h}}}(\bar{s}) = C_{m_{\bar{h}}} + \sum_{i=1}^{6} \frac{g_i}{\bar{s} - v_i} \tag{63}$$

where $\bar{s} = ik = \frac{i\omega c}{2V_\infty}$ is the non-dimensional Laplace variable.

The quantities $C_{L_{\ddot{\alpha}}}$, $C_{L_{\dot{\alpha}}}$, $C_{m_{\ddot{\alpha}}}$, and $C_{m_{\dot{\alpha}}}$ are the dynamic stability derivatives of the lift and pitching moment coefficients with respect to the angle of attack. The derivatives $C_{L_{\ddot{\alpha}}}$ and $C_{m_{\ddot{\alpha}}}$ are due to the apparent mass effect. The derivatives $C_{L_{\dot{\alpha}}}$, $C_{m_{\dot{\alpha}}}$, $C_{L_{\dot{h}}}$, and $C_{m_{\dot{h}}}$represent the aerodynamic damping due to the changes in the angle of attack and the altitude rate. The rational fractions provide the additional poles in the frequency response functions to improve accuracy. It should be noted that the quantities C_{L_α} and C_{m_α} are replaced by the total steady-state stability derivatives for the full aircraft configuration to account for the tail contribution which is usually larger than the wing contribution for the pitching moment.

The rational fraction approximation is performed by a linear regression technique to minimize the error square between the frequency response functions and the rational fraction approximation. For example, the minimization for the frequency response function $C_{L_{\tilde{\alpha}}}$ is described by the cost function

$$J = \frac{1}{2Q}\left[\Re(\varepsilon)\right]^2 + \frac{Q}{2}\left[\Im(\varepsilon)\right]^2 \tag{64}$$

where ε is the approximation error for N data samples generated by an interpolation over a reduced frequency range given by

$$\begin{aligned}
\varepsilon &= \sum_{n=1}^{N}\left(C_{L_{\ddot{\alpha}}}\bar{s}_n^2 + C_{L_{\dot{\alpha}}}\bar{s}_n + C_{L_\alpha} + \sum_{j=1}^{6}\frac{a_j\bar{s}_n}{\bar{s}_n - p_j} - C_{L_{\tilde{\alpha}_n}}\right) \\
&= \sum_{n=1}^{N}\left[-C_{L_{\ddot{\alpha}}}k_n^2 + C_{L_\alpha} + \sum_{j=1}^{6}\frac{a_j k_n^2}{k_n^2 + p_j^2} - \Re\left(C_{L_{\tilde{\alpha}_n}}\right)\right] \\
&\quad + i\sum_{n=1}^{N}\left[C_{L_{\dot{\alpha}}}k_n - \sum_{j=1}^{6}\frac{a_j p_j k_n}{k_n^2 + p_j^2} - \Im\left(C_{L_{\tilde{\alpha}_n}}\right)\right]
\end{aligned} \tag{65}$$

and $Q > 0$ is a weighting coefficient that can be adjusted to give relative accuracy in either the magnitude or phase angle.

The poles p_i, $i = 1,\ldots,6$ are pre-selected to be negative values in the range between 0 and $-k_{max}$ where k_{max} is the largest reduced frequency in the CFD simulation data. The pre-selected values are generated by a random function. The linear regression is repeated over a large number of iterations and the results corresponding to the smallest error are obtained.

The minimization is obtained by taking the partial derivatives of J with respect to $C_{L_{\ddot{\alpha}}}$, $C_{L_{\dot{\alpha}}}$, C_{L_α}, and a_i and setting them to zero. This results in

$$\frac{\partial J}{\partial C_{L_{\ddot{\alpha}}}} = \frac{1}{Q}\Re\left(\bar{s}^2\varepsilon\right) + Q\Im\left(\bar{s}^2\varepsilon\right) \tag{66}$$

$$\frac{\partial J}{\partial C_{L_{\dot{\alpha}}}} = \frac{1}{Q}\Re\left(\bar{s}\varepsilon\right) + Q\Im\left(\bar{s}\varepsilon\right) \tag{67}$$

$$\frac{\partial J}{\partial C_{L_\alpha}} = \frac{1}{Q}\Re\left(\varepsilon\right) + Q\Im\left(\varepsilon\right) \tag{68}$$

$$\frac{\partial J}{\partial C_{a_i}} = \frac{1}{Q}\Re\left(\frac{\bar{s}\varepsilon}{\bar{s} - p_i}\right) + Q\Im\left(\frac{\bar{s}\varepsilon}{\bar{s} - p_i}\right) \tag{69}$$

This results in a linear matrix equation which can be readily solved to obtain $C_{L_{\ddot{\alpha}}}$, $C_{L_{\dot{\alpha}}}$, $C_{L_{\alpha}}$, and a_i

$$\begin{bmatrix} \sum_{n=1}^{N} \frac{k_n^4}{Q} & 0 & -\sum_{n=1}^{N} \frac{k_n^2}{Q} & -\sum_{n=1}^{N} \frac{k_n^2 f_n}{Q} \\ 0 & \sum_{n=1}^{N} Q k_n^2 & 0 & -\sum_{n=1}^{N} Q f_n p \\ -\sum_{n=1}^{N} \frac{k_n^2}{Q} & 0 & \frac{N}{Q} & \sum_{n=1}^{N} \frac{f_n}{Q} \\ -\sum_{n=1}^{N} \frac{k_n^2 f_n^\top}{Q} & -\sum_{n=1}^{N} Q p f_n^\top & \sum_{n=1}^{N} \frac{f_n^\top}{Q} & \sum_{n=1}^{N} \left(\frac{f_n^\top f_n}{Q} + \frac{Q p f_n^\top f_n p}{k_n^2} \right) \end{bmatrix} \begin{bmatrix} C_{L_{\ddot{\alpha}}} \\ C_{L_{\dot{\alpha}}} \\ C_{L_{\alpha}} \\ a \end{bmatrix}$$

$$= \begin{bmatrix} -\sum_{n=1}^{N} \frac{k_n^2 \Re\left(C_{L_{\tilde{\alpha}_n}}\right)}{Q} \\ \sum_{n=1}^{N} Q k_n \Im\left(C_{L_{\tilde{\alpha}_n}}\right) \\ \sum_{n=1}^{N} \frac{\Re\left(C_{L_{\tilde{\alpha}_n}}\right)}{Q} \\ \sum_{n=1}^{N} \left[\frac{f_n^\top \Re\left(C_{L_{\tilde{\alpha}_n}}\right)}{Q} - \frac{Q p f_n^\top \Im\left(C_{L_{\tilde{\alpha}_n}}\right)}{k_n} \right] \end{bmatrix} \tag{70}$$

where $f_n = \begin{bmatrix} \frac{k_n^2}{k_n^2+p_1^2} & \cdots & \frac{k_n^2}{k_n^2+p_6^2} \end{bmatrix}$, $p = \text{diag}\,(p_1, \ldots, p_6)$, and $a = \begin{bmatrix} a_1 & \ldots & a_6 \end{bmatrix}^\top$.

The lift and pitching moment contributions due to the dynamic stability derivatives with respect to the angle of attack and altitude rate are then expressed as

$$\left(C_{L_{\tilde{\alpha}}} - C_{L_{\alpha}}\right) \alpha + \frac{C_{L_{\dot{h}}}}{V_\infty} \dot{h} = \frac{C_{L_{\ddot{\alpha}}} \bar{c}^2}{(2V_\infty)^2} \ddot{\alpha} + \frac{C_{L_{\dot{\alpha}}} \bar{c}}{2V_\infty} \dot{\alpha} + \sum_{j=1}^{6} \eta_j + \frac{C_{L_{\dot{h}}}}{V_\infty} \dot{h} + \sum_{j=1}^{6} \sigma_j \tag{71}$$

$$\left(C_{m_{\tilde{\alpha}}} - C_{m_{\alpha}}\right) \alpha + \frac{C_{m_{\dot{h}}}}{V_\infty} \dot{h} = \frac{C_{m_{\ddot{\alpha}}} \bar{c}^2}{(2V_\infty)^2} \ddot{\alpha} + \frac{C_{m_{\alpha}} \bar{c}}{2V_\infty} \dot{\alpha} + \sum_{j=1}^{6} \nu_j + \frac{C_{m_h}}{V_\infty} \dot{h} + \sum_{j=1}^{6} \mu_j \tag{72}$$

where μ_j, ν_j, σ_j, and μ_j are the unsteady aerodynamic states for the lift and pitching moment coefficients due to the angle of attack and the altitude rate and are described by the following equations:

$$\frac{\bar{c}}{2V_\infty} \dot{\eta}_j = p_j \eta_j + \frac{a_j \bar{c}}{2V_\infty} \dot{\alpha} \tag{73}$$

$$\frac{\bar{c}}{2V_\infty} \dot{\nu}_j = q_j \nu_j + \frac{b_j \bar{c}}{2V_\infty} \dot{\alpha} \tag{74}$$

$$\frac{\bar{c}}{2V_\infty} \dot{\sigma}_j = u_j \sigma_j + \frac{f_j}{V_\infty} \dot{h} \tag{75}$$

$$\frac{\bar{c}}{2V_\infty} \dot{\mu}_j = v_j \sigma_j + \frac{g_j}{V_\infty} \dot{h} \tag{76}$$

Figures 18(a)-(b) show the frequency response functions of the dynamic stability derivatives of the lift and pitching moment coefficients with respect to the angle of attack, respectively. Figures 19(a)-(b) show the frequency response functions of the dynamic stability derivatives of the lift and pitching moment coefficients with respect to the altitude rate, respectively.

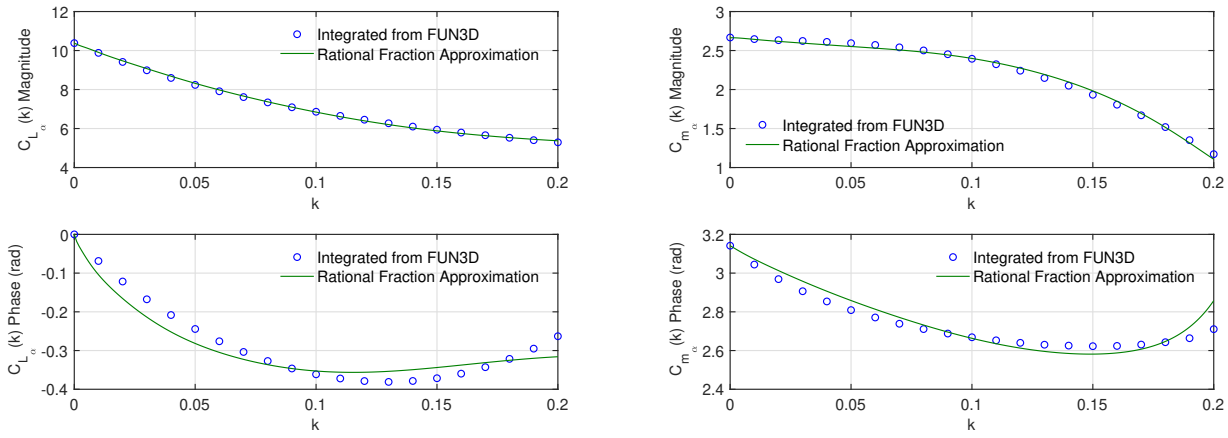

(a) (b)

Figure 18. Mach 0.745 Transonic Truss-Braced Wing C_{L_α} and C_{m_α} Frequency Response Functions

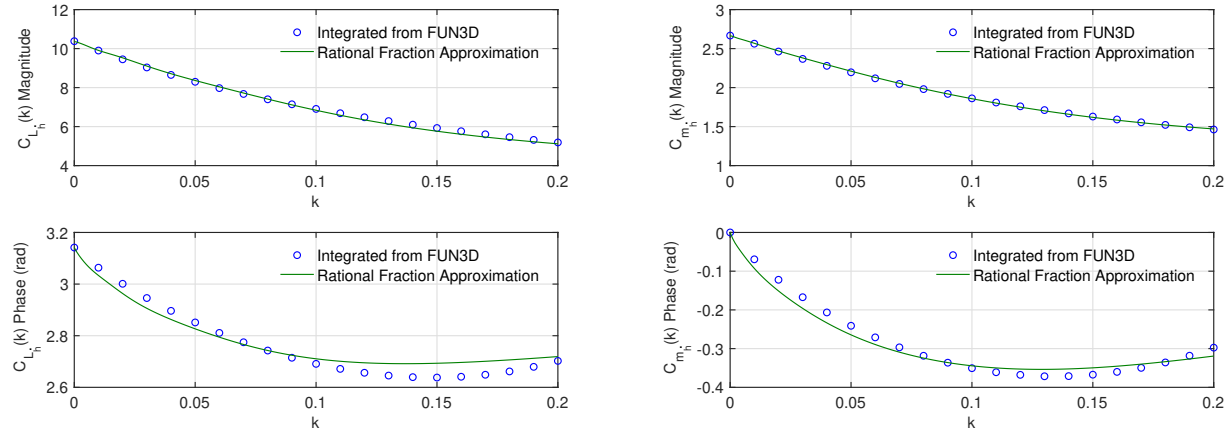

(a) (b)

Figure 19. Mach 0.745 Transonic Truss-Braced Wing $C_{L_{\dot{h}}}$ and $C_{m_{\dot{h}}}$ Frequency Response Functions

B. Dynamic Stability Derivatives with Respect to Pitch Rate

The pitch rate creates an effective plunge velocity at the three-quarter chord collation point on an airfoil

$$\dot{h}_c = q\left(x_c - x_{cg}\right) \tag{77}$$

where x_c is the effective downwash three-quarter chord location.

The incremental lift and lift coefficient are computed as

$$\Delta L = q_\infty \int_{\frac{-b}{2}}^{\frac{b}{2}} c_{l_{\dot{h}}}\left(x_c - x_{cg}\right) c\,dy$$

$$\Delta C_L = \frac{\Delta L}{q_\infty S} = \frac{q\bar{c}}{2V_\infty}\frac{2}{S\bar{c}}\int_{\frac{-b}{2}}^{\frac{b}{2}} c_{l_{\dot{h}}}\left(x_c - x_{cg}\right) c\,dy \tag{78}$$

The lift derivative is then obtained as

$$C_{L_{\tilde{q}}} = \frac{\partial \Delta C_L}{\partial \left(\frac{q\bar{c}}{2V_\infty}\right)} = \frac{2}{S\bar{c}} \int_{\frac{-b}{2}}^{\frac{b}{2}} c_{l_{\frac{\dot{z}}{h}}} \left(x_c - x_{cg}\right) c dy \tag{79}$$

The incremental pitching moment and pitching moment coefficient are computed as

$$\Delta m = q_\infty \int_{\frac{-b}{2}}^{\frac{b}{2}} \left[c_{m_{\frac{\dot{z}}{h}}} \frac{q}{V_\infty} \left(x_c - x_{cg}\right) c + c_{l_{\frac{\dot{z}}{h}}} \frac{q}{V_\infty} \left(x_c - x_{cg}\right) \left(x_{cg} - x_a\right) \right] c dy \tag{80}$$

$$\Delta C_m = \frac{\Delta m}{q_\infty S\bar{c}} = \frac{q\bar{c}}{2V_\infty} \frac{2}{S\bar{c}^2} \int_{\frac{-b}{2}}^{\frac{b}{2}} \left[c_{m_{\frac{\dot{z}}{h}}} \left(x_c - x_{cg}\right) c + c_{l_{\frac{\dot{z}}{h}}} \left(x_c - x_{cg}\right) \left(x_{cg} - x_a\right) \right] c dy \tag{81}$$

The pitching moment derivative is obtained as

$$C_{m_{\tilde{q}}} = \frac{\partial \Delta C_m}{\partial \left(\frac{q\bar{c}}{2V_\infty}\right)} = \frac{2}{S\bar{c}^2} \int_{\frac{-b}{2}}^{\frac{b}{2}} \left[c_{m_{\frac{\dot{z}}{h}}} \left(x_c - x_{cg}\right) c + c_{l_{\frac{\dot{z}}{h}}} \left(x_c - x_{cg}\right) \left(x_{cg} - x_a\right) \right] c dy \tag{82}$$

The frequency response functions of the lift and pitching moment derivatives with respect to the pitch rate are then approximated as

$$C_{L_{\tilde{q}}}(\bar{s}) = C_{L_{\dot{q}}} \bar{s} + C_{L_q} + \sum_{j=1}^{6} \frac{c_j \bar{s}}{\bar{s} - r_j} \tag{83}$$

$$C_{m_{\tilde{q}}}(\bar{s}) = C_{m_{\dot{q}}} \bar{s} + C_{m_q} + \sum_{j=1}^{6} \frac{d_j \bar{s}}{\bar{s} - s_j} \tag{84}$$

where $C_{L_{\dot{q}}}$ and $C_{m_{\dot{q}}}$ are the dynamic stability derivatives of the lift and pitching moment coefficients due to the pitch acceleration.

The lift and pitching moment contributions due to the dynamic stability derivatives with respect to the pitch rate are then expressed as

$$\frac{\left(C_{L_{\tilde{q}}} - C_{L_q}\right)\bar{c}}{2V_\infty} q = \frac{C_{L_{\dot{q}}} \bar{c}^2}{\left(2V_\infty\right)^2} \dot{q} + \sum_{j=1}^{6} \lambda_j \tag{85}$$

$$\frac{\left(C_{m_{\tilde{q}}} - C_{m_q}\right)\bar{c}}{2V_\infty} q = \frac{C_{m_{\dot{q}}} \bar{c}^2}{\left(2V_\infty\right)^2} \dot{q} + \sum_{j=1}^{6} \kappa_j \tag{86}$$

where λ_j and κ_j are the unsteady aerodynamic states for the lift and pitching moment coefficients due to the pitch rate and are described by the following equations:

$$\frac{\bar{c}}{2V_\infty} \dot{\lambda}_j = r_j \lambda_j + \frac{c_j \bar{c}^2}{\left(2V_\infty\right)^2} \dot{q} \tag{87}$$

$$\frac{\bar{c}}{2V_\infty} \dot{\kappa}_j = s_j \kappa_j + \frac{d_j \bar{c}^2}{\left(2V_\infty\right)^2} \dot{q} \tag{88}$$

Figures 20(a) and (b) show the frequency response functions of the dynamic stability derivatives of the lift and pitching moment coefficients with respect to the pitch rate, respectively.

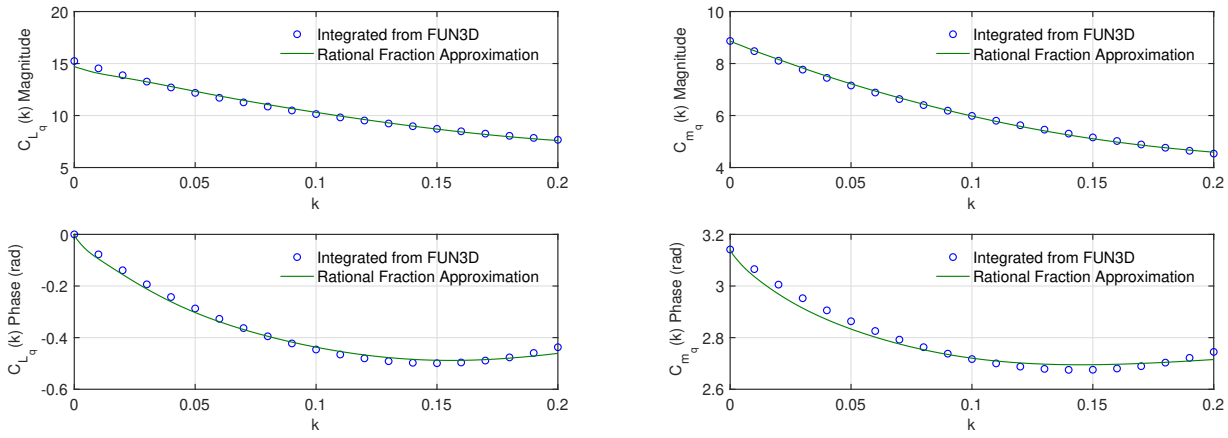

(a) (b)

Figure 20. Mach 0.745 Transonic Truss-Braced Wing $C_{L_{\tilde{q}}}$ and $C_{m_{\tilde{q}}}$ Frequency Response Functions

C. Dynamic Stability Derivatives with Respect to Roll Rate

The roll rate creates an effective plunge velocity along the wing span

$$\dot{h}_c = py \tag{89}$$

The incremental rolling moment and rolling moment coefficient are computed as

$$\Delta l = -q_\infty \int_{\frac{-b}{2}}^{\frac{b}{2}} c_{l_{\dot{h}}} \frac{py^2}{V_\infty} c dy \tag{90}$$

$$\Delta C_l = \frac{\Delta l}{q_\infty S b} = -\frac{pb}{2V_\infty} \frac{2}{Sb^2} \int_{\frac{-b}{2}}^{\frac{b}{2}} c_{l_{\dot{h}}} y^2 c dy \tag{91}$$

The rolling moment derivative is obtained as

$$C_{l_{\tilde{p}}} = \frac{\partial \Delta C_l}{\partial \left(\frac{pb}{2V_\infty}\right)} = -\frac{2}{Sb^2} \int_{\frac{-b}{2}}^{\frac{b}{2}} c_{l_{\dot{h}}} y^2 c dy \tag{92}$$

The frequency response function of the rolling moment derivative with respect to the pitch rate are then approximated as

$$C_{l_{\tilde{p}}}(\bar{s}) = C_{l_{\dot{p}}} \bar{s} + C_{l_p} + \sum_{j=1}^{6} \frac{e_j \bar{s}}{\bar{s} - t_j} \tag{93}$$

The rolling moment contribution due to the dynamic stability derivative with respect to the roll rate is then expressed as

$$\frac{\left(C_{l_{\tilde{p}}} - C_{l_p}\right) b}{2V_\infty} p = \frac{C_{l_{\dot{p}}} b \bar{c}}{(2V_\infty)^2} \dot{p} + \sum_{j=1}^{6} \xi_j \tag{94}$$

where ξ_j is the unsteady aerodynamic state for the rolling moment coefficient due to the roll rate and is described by the following equation:

$$\frac{\bar{c}}{2V_\infty} \dot{\xi}_j = t_j \xi_j + \frac{e_j b \bar{c}}{(2V_\infty)^2} \dot{p} \tag{95}$$

Figure 21 shows the the frequency response function of the dynamic stability derivative of the rolling moment coefficient with respect to the roll rate.

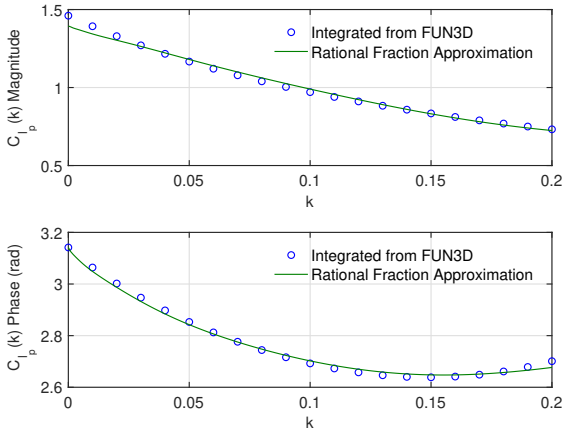

Figure 21. Mach 0.745 Transonic Truss-Braced Wing $C_{l_{\bar{p}}}$ Frequency Response Function

D. Dynamic Stability Derivatives with Respect to Yaw Rate

The yaw rate an effective incremental airspeed along the wing span as

$$\Delta V_\infty = -ry \tag{96}$$

This results in the effective angle of attack

$$\alpha_c = \alpha \frac{ry}{V_\infty} \tag{97}$$

The incremental rolling moment is computed as

$$\begin{aligned}
\Delta l &= -\int_{\frac{-b}{2}}^{\frac{b}{2}} c_{l_{\tilde{\alpha}}} \left(\alpha + \alpha \frac{ry}{V_\infty}\right) \frac{1}{2}\rho_\infty \left(V_\infty - ry\right)^2 ycdy + \int_{\frac{-b}{2}}^{\frac{b}{2}} c_{l_{\tilde{\alpha}}} \alpha \frac{1}{2}\rho_\infty V_\infty^2 ycdy \\
&= -\int_{\frac{-b}{2}}^{\frac{b}{2}} c_{l_{\tilde{\alpha}}} \alpha \frac{1}{2}\rho_\infty \left(-2V_\infty ry + r^2y^2\right) ycdy - \int_{\frac{-b}{2}}^{\frac{b}{2}} c_{l_{\tilde{\alpha}}} \alpha \frac{ry}{V_\infty} \frac{1}{2}\rho_\infty \left(V_\infty - ry\right)^2 ycdy \\
&= q_\infty \int_{\frac{-b}{2}}^{\frac{b}{2}} c_{l_{\tilde{\alpha}}} \frac{\alpha r y^2}{V_\infty} cdy - q_\infty \int_{\frac{-b}{2}}^{\frac{b}{2}} c_{l_\alpha} \frac{\alpha r^3 y^4}{V_\infty^3} cdy
\end{aligned} \tag{98}$$

Note that the integrals that contain y and y^3 are zero in the evaluation of the incremental yawing moment due to the assumption of symmetric $c_{l_{\tilde{\alpha}}}$. Since the term with V_∞^3 is smaller, it can be neglected. The incremental rolling coefficient is then computed as

$$\Delta C_l = \frac{\Delta l}{q_\infty Sb} = \frac{rb}{2V_\infty} \frac{2}{Sb^2} \int_{\frac{-b}{2}}^{\frac{b}{2}} c_{l_\alpha} \alpha y^2 cdy \tag{99}$$

The rolling moment derivative is then obtained as

$$C_{l_{\bar{r}}} = \frac{\partial \Delta C_l}{\partial \left(\frac{rb}{2V_\infty}\right)} = \frac{2}{Sb^2} \int_{\frac{-b}{2}}^{\frac{b}{2}} c_{l_\alpha} \alpha y^2 cdy \tag{100}$$

The frequency response function of the rolling moment derivative with respect to the yaw rate are then approximated as

$$C_{l_{\bar{r}}}(\bar{s}) = C_{l_{\dot{r}}} \bar{s} + C_{l_r} + \sum_{j=1}^{6} \frac{h_j \bar{s}}{\bar{s} - w_j} \tag{101}$$

The rolling moment contribution due to the dynamic stability derivative with respect to the yaw rate is then expressed as

$$\frac{(C_{l_{\bar{r}}} - C_{l_r})\, b}{2V_\infty} r = \frac{C_{l_{\dot{r}}} b\bar{c}}{(2V_\infty)^2}\dot{r} + \sum_{j=1}^{6} \zeta_j \tag{102}$$

where ξ_j is the unsteady aerodynamic state for the rolling moment coefficient due to the roll rate and is described by the following equation:

$$\frac{\bar{c}}{2V_\infty}\dot{\zeta}_j = w_j \zeta_j + \frac{h_j b\bar{c}}{(2V_\infty)^2}\dot{r} \tag{103}$$

Figure 22 shows the the frequency response function of the dynamic stability derivative of the rolling moment coefficient with respect to the yaw rate.

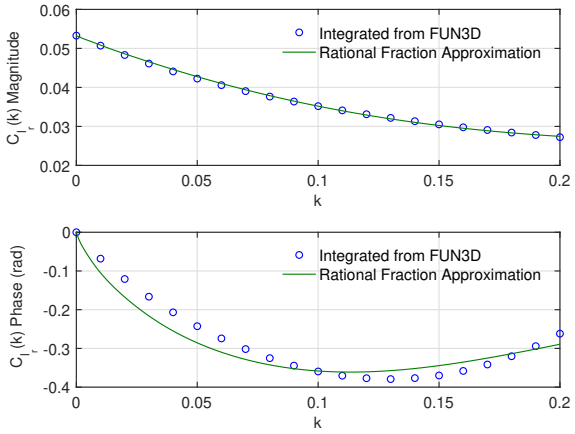

Figure 22. Mach 0.745 Transonic Truss-Braced Wing $C_{l_{\bar{r}}}$ Frequency Response Function

V. Flight Dynamic Stability Analysis

To conduct the flight dynamic stability analysis of the Mach 0.745 TTBW, we obtain the linearized equations of motion of the aircraft in the stability axes about the trim level flight at the trim angle of attack $\bar{\alpha}$.

The linearized equations of motion for longitudinal dynamics are governed by

$$\dot{h} = V_\infty(\theta - \alpha) \tag{104}$$

$$\dot{\theta} = q \tag{105}$$

$$m\dot{V} = -C_D q_\infty S - mg(\theta - \alpha) \tag{106}$$

$$mV_\infty\dot{\alpha} = -C_L q_\infty S + mV_\infty q \tag{107}$$

$$I_{yy}\dot{q} = C_m q_\infty S\bar{c} \tag{108}$$

The linearized equations of motion for lateral-directional dynamics are governed by

$$\dot{\phi} = p \tag{109}$$

$$mV_\infty\dot{\beta} = C_y q_\infty S + mg\phi + mV(\bar{\alpha}p - r) \tag{110}$$

$$I_{xx}\dot{p} - I_{xz}\dot{r} = C_l q_\infty Sb \tag{111}$$

$$-I_{xz}\dot{p} + I_{zz}\dot{r} = C_n q_\infty Sb \tag{112}$$

The trim condition is at Mach 0.745 and the altitude of 43,606 ft corresponding to the trim lift coefficient $\bar{C}_L = 0.73$ which is the design lift coefficient of the Mach 0.745 TTBW. The results for VSPAERO without the transonic corrections are presented in Table 1. The VSPAERO steady-state stability derivatives do not account for transonic correction. The short-period mode is stable but the eigenvalues of the phugoid and plunge modes indicate instability. The damping of the Dutch-roll mode is 3.6% which is unacceptable. Both the roll and spiral modes are stable.

Mode	Eigenvalue	Frequency (rad/sec)	Damping Ratio
Short-Period	$-0.3578 \pm 0.3461i$	0.4978	0.7188
Phugoid	$0.004054 \pm 0.06248i$	0.06261	-0.06475
Plunge	0.0001929		
Dutch-Roll	$-0.008303 \pm 0.2278i$	0.2279	0.03643
Roll	-0.4902		
Spiral	-0.0007362		

Table 1. Eigenvalues of Flight Dynamic Modes of Mach 0.745 Transonic Truss-Braced Wing without Transonic Correction

Table 2 presents the eigenvalues of the flight dynamic modes with the transonic correction of the steady-state stability derivatives computed by VSPAERO. The transonic correction is computed by the transonic small disturbance (TSD) code TSFOIL.[10] This code is loosely coupled to an in-house integral boundary layer (IBL) code to correct for the viscous flow interaction with the transonic shock on an airfoil.[11] The increase in the wave drag evidently results in the increase in the drag stability derivative which contributes to the airspeed damping. As a result, the phugoid and the plunge modes are both stable.

Mode	Eigenvalue	Frequency (rad/sec)	Damping Ratio
Short-Period	$-0.3676 \pm 0.3346i$	0.4971	0.7396
Phugoid	$-0.008282 \pm 0.07693i$	0.07738	0.1070
Plunge	-0.008621		
Dutch-Roll	$-0.005294 \pm 0.2266i$	0.2267	0.02336
Roll	-0.4950		
Spiral	-0.001945		

Table 2. Eigenvalues of Flight Dynamic Modes of Mach 0.745 Transonic Truss-Braced Wing with Transonic-Corrected Steady-State Stability Derivatives

Table 3 presents the eigenvalues of the flight dynamic modes with both the transonic-corrected steady-state and dynamic stability derivatives. There are 42 eigenvalues. Only those eigenvalues associated with the flight dynamic modes are shown. Comparing the results with only the transonic-corrected steady-state stability derivatives, the dynamic stability derivatives contribute more damping to some of the flight dynamic modes such as the phugoid mode and the Dutch-roll modes.

Mode	Eigenvalue	Frequency (Hz)	Damping Ratio
Short-Period	$-0.07317 \pm 0.2183i$	0.2303	0.3178
Phugoid	$-0.3483,\ -0.07580$	0.1625	1.3050
Plunge	-0.002748		
Dutch-Roll	$-0.01410 \pm 0.2049i$	0.2054	0.06865
Roll	-0.2736		
Spiral	-0.002282		

Table 3. Eigenvalues of Flight Dynamic Modes of Mach 0.745 Transonic Truss-Braced Wing with Transonic-Corrected Steady-State and Dynamic Stability Derivatives

To illustrate the effect of transonic aerodynamics on flight dynamic stability, two simulations are conducted with

an initial angle of attack of 1° for the longitudinal motion and an initial angle of sideslip of 1° for the lateral-directional motion. Figures 23(a)-(d) show the angle of attack, pitch rate, airspeed, and altitude, respectively. Without the transonic steady-state and dynamic stability derivatives, the longitudal motion is divergent. With only the transonic steady-state stability derivatives, the motion becomes stable but the response can be seen to be oscillatory for up to 300 sec. This would be highly objectionable from the handling qualities and ride quality perspectives. The effect of the transonic dynamic stability derivatives is apparent as the motion becomes much more stable and no longer exhibits sustained oscillations. However, some large transients in the angle of attack and pitch rate are observed.

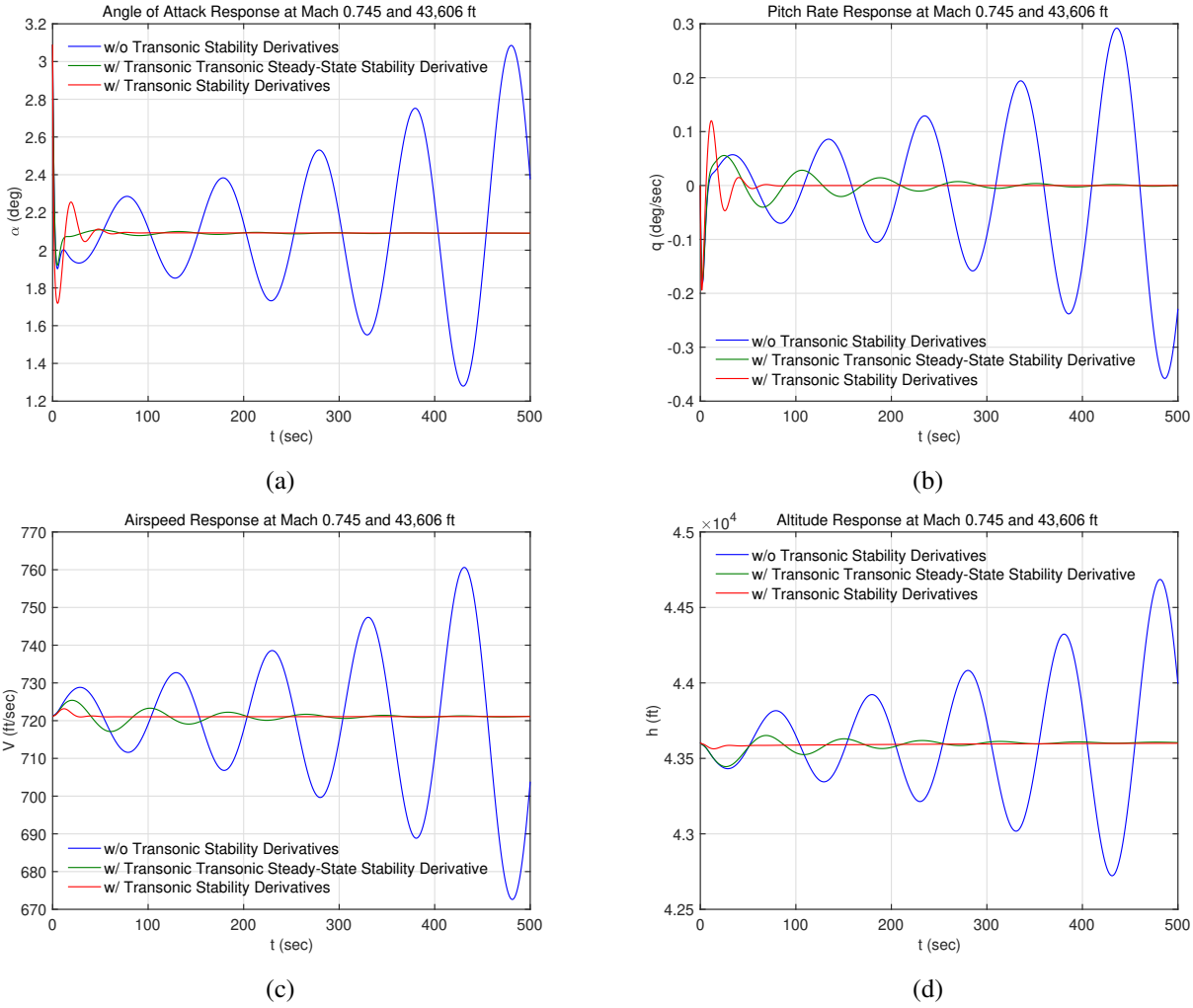

Figure 23. Mach 0.745 Transonic Truss-Braced Wing Longitudinal Dynamic Response to Initial 1° Angle of Attack

Figure 24(a)-(d) show the roll angle, roll rate, angle of sideslip, and the yaw rate, respectively. The effect of the transonic dynamic stability derivatives can be readily seen as the lateral-directional motion becomes more damped than the motions computed without the transonic correction and with only the steady-state stability derivatives.

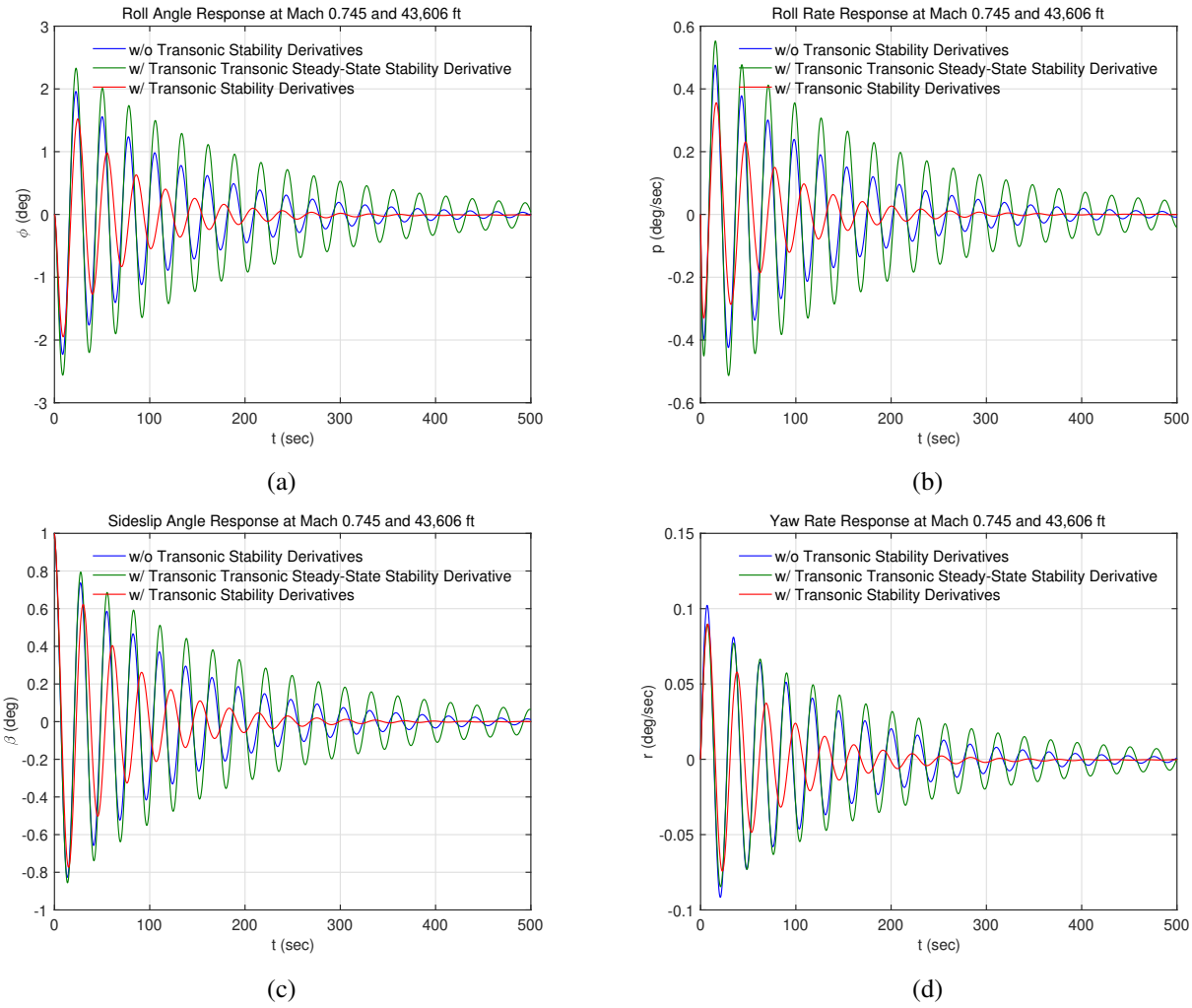

Figure 24. Mach 0.745 Transonic Truss-Braced Wing Lateral-Directional Dynamic Response to Initial 1° Angle of Sideslip

VI. Discussion

This study points out the significance of the role of transonic aerodynamics on the dynamic stability of the Mach 0.745 TTBW. Lower-order tools for assessing flight dynamic stability usually do not have capabilities for predicting transonic aerodynamics. This could result in incorrect estimation of the stability derivatives which could lead to inaccurate stability assessments. By correcting transonic aerodynamics in the steady-state derivatives, improvements in the stability derivatives can be obtained but are still insufficient to accurately capture the dynamic stability. Transonic correction to steady-state stability derivatives can be implemented fairly readily to coupling steady-state transonic flow solvers to lower-order tools, or simply by correcting using the lift curve slopes obtained from high-fidelity steady-state CFD simulations.

Transonic dynamic stability analysis is much more complex and require unsteady RANS simulations which are computationally expensive. Conducting full three-dimensional unsteady RANS simulations is usually prohibitive. In this study, we develop an approach for analyzing the transonic stability derivatives using a transonic correction method developed for the Theodorsen's theory. This method has been shown to be able to accurately capture the nonlinear unsteady transonic aerodynamics due to the moving shock. The method is leveraged to compute the frequency response functions of the lift and pitching moment derivatives. The transonic dynamic stability derivatives are then obtained from the frequency response functions by a rational fraction approximation.

With respect to the Mach 0.745 TTBW, an initial flight dynamic stability analysis has been conducted. The analysis

shows that the aircraft has all stable flight dynamic modes when the transonic dynamic stability derivatives are included in the analysis. However, the frequencies and damping values of the short-period mode and Dutch-roll mode are not considered acceptable from a handling qualities perspective. In particular, it is observed that the frequencies of the short-period mode and the Dutch-roll mode appear to be too low. Typical frequencies of the short-period mode and the Dutch-roll mode usually about an order or magnitude larger. While the damping can be improved with a flight control system, the frequencies cannot usually be raised substantially by the flight control system alone. A further examination of the mass and inertia properties may be necessary to refine the stability analysis.

VII. Conclusions

This study develops a method for dynamic stability analysis that captures the transonic aerodynamics of the Mach 0.745 Transonic Truss-Braced Wing aircraft. The method leverages a recently developed transonic correction method for unsteady transonic aerodynamics. This method is shown to be able to accurately model the nonlinear unsteady transonic flow associated with a moving shock structure. The dynamic stability analysis method presents techniques for estimating the dynamic stability derivatives by a rational fraction approximation of the frequency response functions of the stability derivatives of the lift, pitching, and rolling moment coefficients with respect to the angle of attack, pitch rate, roll rate, and yaw rates.

The effect of the transonic dynamic stability derivatives is seen as a significant effect in the flight dynamic stability assessments of the Mach 0.745 Transonic Truss-Braced Wing aircraft. In generally, the transonic dynamic stability derivatives contribute substantially to the damping of the flight dynamic modes, thereby improving the dynamic stability of the Mach 0.745 Transonic Truss-Braced Wing aircraft.

The initial dynamic stability analysis indicates that while the all the flight dynamic modes are stable the frequencies and damping values of the short-period mode and the Dutch-roll mode are considered unacceptable from a handing qualities perspective as the frequencies appear to be too low. A future dynamic stability study will be conducted for the Mach 0.8 Transonic Truss-Braced Wing Aircraft.

Acknowledgment

The authors wish to acknowledge NASA Advanced Air Transport Technology project for the funding support of this work. The authors also acknowledge Boeing Research and Technology and in particular Christopher Droney, Neal Harrison, Michael Beyar, Eric Dickey, and Anthony Sclafani, along with the NASA technical POC, Gregory Gatlin, for their research conducted under the NASA BAART contracts NNL10AA05B and NNL16AA04B. The research published in this paper is made possible by the technical data and wind tunnel test data furnished under these BAART contracts.

References

[1]Bradley, M. K. and Droney, C. K., "Subsonic Ultra Green Aircraft Research: Phase I Final Report," NASA Contractor Report NASA/CR-2011-216847, Boeing Research and Technology, April 2011.

[2]Bradley, M. K., Droney, C. K., and Allen, T. J., "Subsonic Ultra Green Aircraft Research Phase II: N+4 Advanced Concept Development," NASA Contractor Report NASA/CR-2012-217556, Boeing Research and Technology, May 2012.

[3]Theodorsen, T., "General Theory of Aerodynamic Instability and the mechanism of Flutter", NACA Report No. 496, 1949.

[4]Nguyen, N., Fugate, J., Kaul, U., and Xiong, J., "Flutter Analysis of the Transonic Truss-Braced Wing Aircraft Using Transonic Correction," AIAA Structural Dynamics Conference, AIAA-2019-0217, January 2019.

[5]Kaul, U. and Nguyen, N., "RANS Simulations of a Pitching and Plunging VCCTEF Airfoil Toward a Transonic Flutter Model," AIAA Structural Dynamics Conference, AIAA-2019-2037, January 2019.

[6]Kaul, U. and Nguyen, N., "Extending A Correction Method for Unsteady Transonic Aerodynamics as Applied to Variable Camber Continuous Trailing Edge Flap," AIAA Applied Aerodynamic Conference, AIAA-2019-3157, June 2019.

[7]Nguyen, N. and Xiong, J., "Transonic Correction to Theodorsen's Theory for Oscillating Airfoil in Pitch and Plunge Toward Flutter," AIAA Structural Dynamics Conference, AIAA-2021-1913, January 2021.

[8]Abel, I., "An Analytical Technique for Predicting the Characteristics of a Flexible Wing Equipped with an Active Flutter-Suppression System and Comparison with Wind-Tunnel Data," NASA TP-1367, 1979.

[9]Roger, K. L., "Airplane Math Modeling and Active Aeroelastic Control Design," AGARD CP-228, 1977.

[10]Stahara, S. S., "Operational Manual for Two-Dimensional Transonic Code TSFOIL," NASA Contractor Report 3064, December, 1978.

[11]Fujiwara, G., Chaparro, D., and Nguyen, N., "An Integral Boundary Layer Direct Method Applied to 2D Transonic Small-Disturbance Equations," 34th AIAA Applied Aerodynamics Conference, AIAA-2016-3160, June 2016.